Journal of Computational Physics 336 (2017) 1–35

Contents lists available at ScienceDirect

Journal of Computational Physics

www.elsevier.com/locate/jcp

Non-deteriorating time domain numerical algorithms for Maxwell's electrodynamics ☆

S. Petropavlovsky [a,b], S. Tsynkov [b,c,*]

[a] National Research University Higher School of Economics, Moscow 101000, Russia
[b] Department of Mathematics, North Carolina State University, Box 8205, Raleigh, NC 27695, USA
[c] Moscow Institute of Physics and Technology, Dolgoprudny 141700, Russia

ARTICLE INFO

Article history:
Received 2 September 2016
Received in revised form 27 January 2017
Accepted 29 January 2017
Available online 2 February 2017

Keywords:
Unsteady electromagnetic waves
Maxwell's equations
Unbounded regions
Grid truncation
Artificial outer boundaries
Artificial boundary conditions (ABCs)
Non-reflecting boundaries
Perfectly matched layer (PML)
Long time deterioration
Loss of accuracy, loss of stability, error build-up
The Huygens' principle
Aft fronts of the waves
Lacunae of the solutions
Quasi-lacunae
Accumulation of charge
Guaranteed accuracy
Temporally uniform error bounds

ABSTRACT

The Huygens' principle and lacunae can help construct efficient far-field closures for the numerical simulation of unsteady waves propagating over unbounded regions. Those closures can be either standalone or combined with other techniques for the treatment of artificial outer boundaries. A standalone lacunae-based closure can be thought of as a special artificial boundary condition (ABC) that is provably free from any error associated with the domain truncation. If combined with a different type of ABC or a perfectly matched layer (PML), a lacunae-based approach can help remove any long-time deterioration (e.g., instability) that arises at the outer boundary regardless of why it occurs in the first place.

A specific difficulty associated with Maxwell's equations of electromagnetism is that in general their solutions do not have classical lacunae and rather have quasi-lacunae. Unlike in the classical case, the field inside the quasi-lacunae is not zero; instead, there is an electrostatic solution driven by the electric charges that accumulate over time. In our previous work [23], we have shown that quasi-lacunae can also be used for building the far-field closures. However, for achieving a provably non-deteriorating performance over arbitrarily long time intervals, the accumulated charges need to be known ahead of time.

The main contribution of the current paper is that we remove this limitation and modify the algorithm in such a way that one can rather avoid the accumulation of charge all together. Accordingly, the field inside the quasi-lacunae becomes equal to zero, which facilitates obtaining the temporally uniform error estimates as in the case of classical lacunae. The performance of the modified algorithm is corroborated by a series of numerical simulations. The range of problems that the new method can address includes important combined formulations, for which the interior subproblem may be non-Huygens', and only the exterior subproblem, i.e., the far field, is Huygens'.

☆ Work supported by the US Army Research Office (ARO) under grants # W911NF-14-C-0161 and # W911NF-16-1-0115, and by the US–Israel Binational Science Foundation (BSF) under grant # 2014048.

* Corresponding author at: North Carolina State University, Box 8205, Raleigh, NC 27695, USA.
E-mail addresses: spetrop@ncsu.edu (S. Petropavlovsky), tsynkov@math.ncsu.edu (S. Tsynkov).
URL: http://www4.ncsu.edu/~stsynkov/ (S. Tsynkov).

http://dx.doi.org/10.1016/j.jcp.2017.01.068
0021-9991/

1. Introduction

In this paper, we develop and test a new algorithm that can furnish an exact artificial boundary condition (ABC) for the numerical simulation of electromagnetic waves propagating over unbounded regions, and can also stabilize any existing ABC or PML (perfectly matched layer) on arbitrarily long time intervals. The algorithm applies to a broad range of problems on $\mathbb{R}^3$ that may involve some sophisticated physical phenomena in the near field (generation, absorption, reflection, scattering, etc. of waves inside a bounded region) yet reduce to the propagation of electromagnetic waves in vacuum in the far field. In practice, only the near-field solution is actually computed, while the far field is truncated off and replaced by an ABC or a PML at the artificial outer boundary. The overall problem on $\mathbb{R}^3$ must be uniquely solvable and well-posed.

It is well known that many existing ABCs/PMLs are prone to error growth/instabilities in long-time simulations [1–18]. These undesirable phenomena may be due to continuous ill-posedness or weak well-posedness, discrete instability of a well-posed continuous problem, geometric issues such as near-edge or near-corner implementation of an ABC/PML, etc. Often, specific reasons for the deterioration are not known. This warrants the development of a general approach that can improve the long-time behavior of various methods.

A key advantage of our proposed algorithm is precisely its universality. It treats any given ABC or PML in the same manner and eliminates the need of finding out what actually causes the long-time deterioration in every particular case. The only limitation is that the chosen ABC or PML must be able to maintain its acceptable stable performance over reasonably long periods of time.[1] Those intervals of table performance can still be much shorter than the overall simulation time. An estimate (lower bound) for the interval of stable performance is needed for choosing the parameters of our algorithm. Other than that, its construction does not require any knowledge of why the performance of the original ABC/PML may deteriorate as the time elapses.

The algorithm is based on the Huygens' principle, or, in other words, it exploits the diffusionless propagation of waves in $\mathbb{R}^3$. Specifically, we use the following property of Maxwell's equations in vacuum: provided that the currents driving the pure Maxwell system are compactly supported in both space and time, the propagating electromagnetic waves have sharp aft (i.e., trailing) fronts, and the solution behind those is electrostatic, i.e., it does not evolve in time any longer. In our work [19], we called the region of space–time occupied by the steady-state solution *a quasi-lacuna* of Maxwell's equations. It generalizes the notion of classical lacunae, for which the solution behind the aft fronts is equal to zero, see [20] and also [21,22]. Once the outgoing waves have left the bounded computational domain, or, equivalently, once the latter entirely falls into the quasi-lacuna, there is no need to further update the fields and the simulation can stop. Hence, if the performance of the given ABC or PML during the corresponding finite time interval is acceptable, no subsequent adverse effects due this ABC or PML will ever arise.

In our work [23], we applied the lacunae-based algorithm to solving Maxwell's equations driven by currents that are compactly supported in space yet operate continuously in time (e.g., radiation of electromagnetic waves by an antenna with a given feed). The key idea is to partition the problem in time into a sequence of individual subproblems. Each of the latter appears driven by the currents that are compactly supported in both space and time. This facilitates the application of quasi-lacunae so that the solution of each subproblem does not need to be advanced in time beyond the point where it reaches the steady state on the domain of interest. Then, the overall solution is assembled by linear superposition. For every given moment of time, there are both steady-state and unsteady terms in the superposition sum that yields the solution. The "lifespan" of each unsteady term on the domain of interest is finite and non-increasing, because the domain size is finite and the propagation speed is finite. Moreover, the number of unsteady terms in the sum may never exceed a certain constant for all times, because the waves that leave the domain no longer need to be taken into account. On the other hand, the number of steady-state terms increases as the time elapses, because the electrostatic components of the solution stay on the computational domain even after it falls into the quasi-lacuna, i.e., after the unsteady waves leave. However, as the currents and charges that drive the Maxwell equations are given, the sum of all electrostatic contributions can be replaced by the electrostatic field at the final moment of time, which needs to be computed only once. Altogether, this yields a temporally uniform error estimate, which we proved in [23] and also corroborated with a series of 3D numerical experiments.

To extend the algorithm further, beyond solving the constant coefficient Maxwell equations driven by known currents, we still use the quasi-lacunae as a core integration tool but supplement them by some additional constructs that make the class of admissible formulations even wider:

(A) The original problem is decomposed into the interior problem (IP) and auxiliary problem (AP). The interior problem corresponds to the aforementioned sophisticated physics in the near field. It is formulated on a bounded domain and may be non-Huygens'. The auxiliary problem is formulated for the pure Maxwell equations on the entire $\mathbb{R}^3$ and is driven by the currents that depend on the solution to the IP. The AP satisfies the Huygens' principle. Solution of the AP provides the required closure for the IP at its outer boundary. The task of setting an ABC/PML is rather switched from the IP to the AP.

[1] The proposed methodology will not work in the case of very rapidly developing instabilities due to the treatment of the artificial outer boundaries. For example, it is not likely to offer a "fix" for the classical GKS-type instabilities.

(B) Lacunae-based integration, which involves partitioning of the problem in time into a sequence of individual subproblems, is now applied to the AP, which is Huygens' and has quasi-lacunae.

In [23], we presented a more general version of the lacunae-based algorithm that incorporated the additional components (A) and (B). However, unlike in the previous case, the currents and charges that drive the AP are not known ahead of time and rather obtained in the course of time marching. Hence, the electrostatic solutions on the domain of interest have to be evaluated numerically for all individual subproblems as the time elapses, and their sum cannot be replaced by one final electrostatic solution. Adding together an increasing number of computed electrostatic solutions may potentially cause a build-up of the error on the computational domain. While in practice it has never been observed, see [23], we still could not rigorously prove a temporally uniform error bound for the lacunae-based algorithm that involved steps (A) and (B). Therefore, in the current work we address this issue by adding one more building block to the algorithm:

(C) The currents that drive the individual subproblems in (B) are modified so that the charge density accumulated during the operational period of any given partial current is equal to zero.[2] It means that the residual electrostatic field behind the aft front of the traveling wave (i.e., inside the quasi-lacuna) becomes zero as well. In other words, the steady-state contributions to the solution of the AP merely vanish. In this sense, quasi-lacunae reduce to classical lacunae, although not in general but only for those specially modified auxiliary currents.

Step (C) is crucial from the viewpoint of theory because it allows one to derive a rigorous temporally uniform error bound which guarantees that the error due to the treatment of the artificial outer boundary will not accumulate over time. This is equivalent to having an algorithm that applies to combined problems of type (A) and has a provably non-deteriorating behavior over arbitrarily long times. We consider it the main contribution of this paper. We also note that this is the same non-deterioration behavior available now for Maxwell's equations that we have obtained previously for the scalar case using classical lacunae of the wave (d'Alembert) equation, see [24–26].

The actual construction of the modified currents in step (C) requires, as a key element, a solenoidal (i.e., divergence-free) extension of the solution from the far field to the near field, i.e., to the interior of the computational domain. We perform it by solving a special auxiliary Neumann problem for the Poisson equation. The extension, however, is not always possible: the flux of the field to be extended (electric or magnetic) must be equal to zero. In Section 6, we discuss what this requirement means in terms of physics, and what kind of constraints on the class of admissible problems it can impose. It turns out that the corresponding constraints appear rather weak. Moreover, the implementation overheads compared to the previous version of the algorithm [23] are small because the aforementioned Poisson problems are solved by FFT.

The remainder of the paper is organized as follows. In Sections 2 and 3, we recall the notion of classical lacunae and quasi-lacunae, respectively. Section 4 presents basic results on the lacunae-based time marching of Maxwell's equations driven by given external currents. In Section 5, we describe the decomposition technique that allows one to use the algorithm for the problems that are non-Huygens' in the near field. Section 6 introduces the modified auxiliary currents that make the residual electrostatic field inside the quasi-lacunae equal to zero. Appendix A provides additional detail of the analysis that supplement the arguments of Section 6. In Section 7, we prove the temporally uniform error bound for the new version of the lacunae-based algorithm. In Section 8, we discuss the implementation details and present the numerical results. Appendix B presents a block diagram of the algorithm. Section 9 contains the conclusions and identifies the directions of future work.

2. Classical lacunae of the wave equation

Consider the inhomogeneous scalar wave (d'Alembert) equation:

$$\frac{1}{c^2}\frac{\partial^2 u}{\partial t^2} - \Delta u = f(\boldsymbol{x}, t), \quad \boldsymbol{x} \in \mathbb{R}^3, \quad t \geq 0, \tag{1}$$

subject to zero initial conditions and with the source term f that is compactly supported on a bounded space–time domain $Q = S \times [0, T_0]$ where $S \subset \mathbb{R}^3$. This means that the source term $f(\boldsymbol{x}, t)$ differs from zero only on S and operates for the limited time interval $[0, T_0]$.

The solution to the Cauchy problem (1) is given by the Kirchhoff integral:

$$u(\boldsymbol{x}, t) = \frac{1}{4\pi} \iiint\limits_{|\boldsymbol{x}-\boldsymbol{\xi}| \leqslant ct} \frac{f(\boldsymbol{\xi}, t - |\boldsymbol{x}-\boldsymbol{\xi}|/c)}{|\boldsymbol{x}-\boldsymbol{\xi}|} d\boldsymbol{\xi}. \tag{2}$$

[2] This operational period is the parameter T_0 in the definition of the partition of unity (28), see also Fig. 5. This parameter is not related to the overall simulation time for the original problem. In practice, T_0 is much shorter and is rather determined by the interval of stable performance of the ABC/PML chosen to terminate the spatial discretization grid. The proposed algorithm in not sensitive to the temporal behavior of the overall solution and can be applied to both genuinely time-dependent simulations, as well as pseudo-time integration.

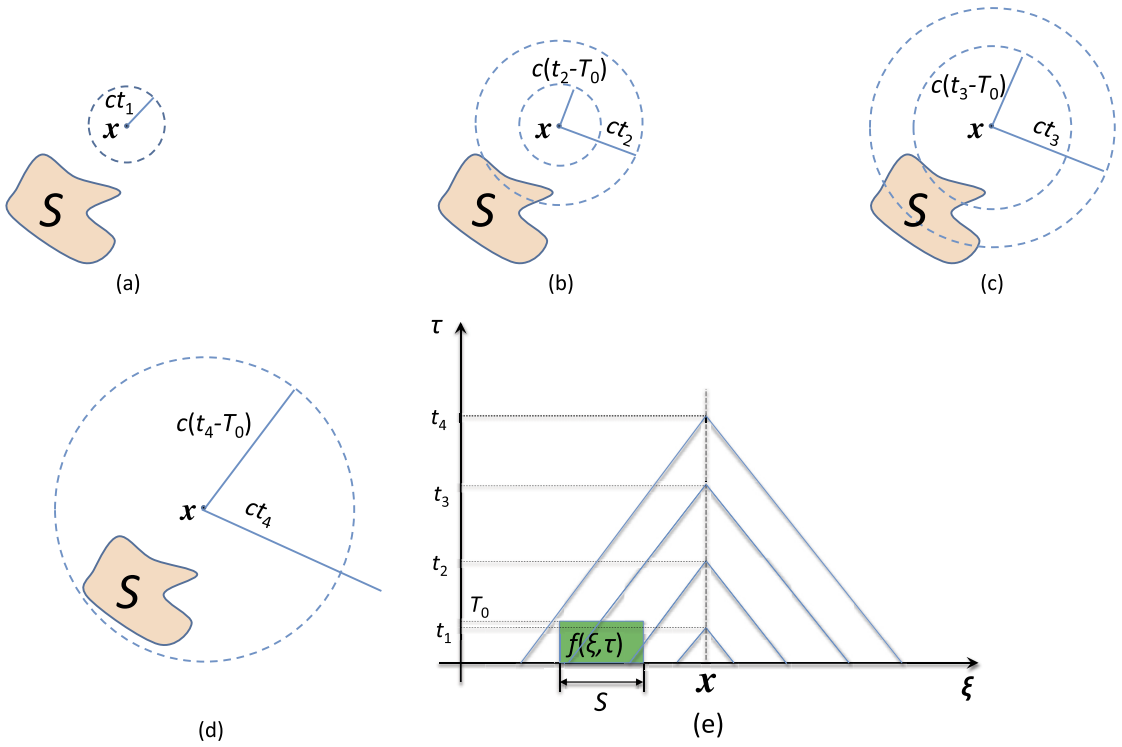

Fig. 1. Visualization of conditions (4) and (5). (For interpretation of the references to color in this figure, the reader is referred to the web version of this article.)

The integration in (2) is performed over the ball of radius ct centered at x. The fact that $f(\boldsymbol{x}, t) = 0$ for $t > T_0$ can be explicitly accounted for in formula (2) by adjusting the domain of integration:

$$u(\boldsymbol{x}, t) = \frac{1}{4\pi} \iiint\limits_{c(t-T_0)\leqslant|\boldsymbol{x}-\boldsymbol{\xi}|\leqslant ct} \frac{f(\boldsymbol{\xi}, t-|\boldsymbol{x}-\boldsymbol{\xi}|/c)}{|\boldsymbol{x}-\boldsymbol{\xi}|} d\boldsymbol{\xi}, \tag{3}$$

which becomes a spherical layer of width cT_0 centered at $\boldsymbol{x}$. This layer continuously expands over time while keeping its width. For sufficiently small times $t < T_0$, it coincides with the ball of radius ct since the inner sphere collapses: $c(t - T_0) < 0$. Note also that as $f(\boldsymbol{x}, t)$ is compactly supported in space on the domain S, a non-zero contribution to the integral (3) occurs only for $\boldsymbol{\xi} \in S$.

When

$$|\boldsymbol{x}-\boldsymbol{\xi}| > ct, \quad \forall \boldsymbol{\xi} \in S, \tag{4}$$

the domain of integration in (3) is empty and hence the integral is zero. Condition (4) defines a spatial domain $\Lambda_0 = \{\boldsymbol{x} | \text{dist}(\boldsymbol{x}, S) > ct\}$ external to S, where $u(\boldsymbol{x}, t) = 0$ at a given moment of time t. From the standpoint of physics, at the time t the domain Λ_0 has not yet been reached by the outgoing waves generated inside S.

On the other hand, after the source ceases to operate at $t = T_0$, the solution $u(\boldsymbol{x}, t)$ is also equal to zero if

$$|\boldsymbol{x}-\boldsymbol{\xi}| < c(t-T_0), \quad \forall \boldsymbol{\xi} \in S, \tag{5}$$

because the domain of integration in (3) is again empty. Therefore, at those moments of time $t > T_0$ for which the constraint (5) holds, there exists another spatial domain:

$$\Lambda_1 = \{\boldsymbol{x} | \, |\boldsymbol{x}-\boldsymbol{\xi}| < c(t-T_0), \, \forall \boldsymbol{\xi} \in S\}, \tag{6}$$

where $u(\boldsymbol{x}, t) = 0$. From the perspective of physics, the domain Λ_1 is the part of space that the waves generated inside S before T_0 have already left by the time t. Conditions (4) and (5) can be illustrated graphically, see Figs. 1(a)–1(d). For a given $\boldsymbol{x}$, the solution $u(\boldsymbol{x}, t)$ is still zero at the time $t = t_1$ (Fig. 1(a)), because the integration area has not reached the support of the integrand S. At later times, $t = t_2$ and $t = t_3$, $u(\boldsymbol{x}, t)$ becomes non-zero as long as the spherical layer $c(t - T_0) \leqslant |\boldsymbol{x} - \boldsymbol{\xi}| \leqslant ct$ overlaps with S (Figs. 1(b) and 1(c)). At even larger times, e.g., $t = t_4$, the solution turns into zero again because the spherical layer expands further and does not intersect with S any longer (Fig. 1(d)). This happens starting from the time t given by

$$\max_{\boldsymbol{\xi}\in S} |\boldsymbol{x}-\boldsymbol{\xi}| = c(t-T_0).$$

We can visualize conditions (4) and (5) in yet another way, introducing the retarded time $\tau = t - \frac{|\boldsymbol{x}-\boldsymbol{\xi}|}{c}$ and recasting the Kirchhoff integral (2) in terms of the variables τ and $\boldsymbol{\xi}$:

$$u(\boldsymbol{x},t) = \frac{1}{4\pi}\int\limits_0^\infty d\tau \iiint\limits_{\mathbb{R}^3} d\boldsymbol{\xi}\frac{f(\boldsymbol{\xi},\tau)}{|\boldsymbol{x}-\boldsymbol{\xi}|}\delta\left(\tau - t + \frac{|\boldsymbol{x}-\boldsymbol{\xi}|}{c}\right). \tag{7}$$

For a given moment of time t and the observation point $\boldsymbol{x}$, the integration in (7) is performed over the surface of the backward characteristic cone with the vertex at $(\boldsymbol{x},t)$, see Fig. 1(e). In the beginning, e.g., at $t = t_1$, the cone does not overlap with the support of $f(\boldsymbol{\xi},\tau)$ (shown in green), so the solution is zero. This corresponds to condition (4), which indicates that the waves have not reached the point $\boldsymbol{x}$ yet. At later times, say, $t = t_2$ or $t = t_3$, the surface of the cone intersects with the support of $f(\boldsymbol{\xi},\tau)$, so $u(\boldsymbol{x},t) \neq 0$. At even larger times, e.g., $t = t_4$, the entire support of $f(\boldsymbol{\xi},\tau)$ is inside the cone, its intersection with the cone's surface is empty, and hence $u(\boldsymbol{x},t) = 0$.

The domains Λ_0 and Λ_1 are the spatial cross-sections of the primary and secondary lacunae of the wave equation at the time t, respectively. The primary lacuna is the part of space–time where the waves generated by a compactly supported source have not reached yet. The secondary lacuna is the part of space–time where the waves have already passed and left a zero background behind the aft fronts. A rigorous definition of the secondary lacuna, which is of central interest for our current work, reads (see [20]):

$$u(\boldsymbol{x},t) \equiv 0 \quad \forall (\boldsymbol{x},t) \in \bigcap_{(\boldsymbol{\xi},\tau)\in Q} \{(\boldsymbol{x},t)\,|\,|\boldsymbol{x}-\boldsymbol{\xi}| < c(t-\tau),\ t > \tau\} \stackrel{\text{def}}{=} \Lambda. \tag{8}$$

The space–time region Λ defined by (8) can be interpreted as the intersection of all forward characteristic cones (i.e., light cones) of the wave equation (1) once the vertex of the cone sweeps the support of the right-hand side $f(\boldsymbol{x},t)$.

The existence of the secondary lacunae and sharp aft fronts is a manifestation of the Huygens' principle, under which the propagation of waves is said to be diffusionless. This phenomenon is inherently three-dimensional (more precisely, it may take place only in spaces of odd dimension $\geqslant 3$), and has been known since Hadamard [27]. The algorithm proposed in the current paper relies on the secondary lacunae for the Maxwell system of equations.

3. Quasi-lacunae of Maxwell's equations

Consider Maxwell's equations:

$$\frac{1}{c}\frac{\partial \boldsymbol{E}}{\partial t} - \operatorname{curl} \boldsymbol{H} = -\frac{4\pi}{c}\boldsymbol{j}, \tag{9}$$

$$\frac{1}{c}\frac{\partial \boldsymbol{H}}{\partial t} + \operatorname{curl} \boldsymbol{E} = -\frac{4\pi}{c}\boldsymbol{j}^M, \tag{10}$$

where $\boldsymbol{E}$ and $\boldsymbol{H}$ are the electric and magnetic field, respectively, and c is the speed of light in vacuum. System (9)–(10) will be solved with zero initial conditions. Equations (9)–(10) are driven by the electric current with density $\boldsymbol{j} = \boldsymbol{j}(\boldsymbol{x},t)$ and magnetic current with density $\boldsymbol{j}^M = \boldsymbol{j}^M(\boldsymbol{x},t)$, although the latter is introduced formally and does not exist in nature. It makes system (9)–(10) symmetric and, more importantly, appears crucial for the analysis of non-Huygens' problems in Section 5. The current densities are related to the respective densities of the electric $\rho = \rho(\boldsymbol{x},t)$ and magnetic $\rho^M = \rho^M(\boldsymbol{x},t)$ charge via the conventional continuity equations:

$$\frac{\partial \rho}{\partial t} + \operatorname{div} \boldsymbol{j} = 0 \quad \text{and} \quad \frac{\partial \rho^M}{\partial t} + \operatorname{div} \boldsymbol{j}^M = 0. \tag{11}$$

According to (11), the charges ρ and ρ^M evolve over time at every spatial location where the currents are non-zero, and hence may accumulate unless the currents are solenoidal, i.e., unless $\operatorname{div} \boldsymbol{j} = 0$ and $\operatorname{div} \boldsymbol{j}^M = 0$. By taking the divergence of both parts of equations (9) and (10) we obtain the expressions that relate the fields to the respective charge densities:

$$\frac{\partial}{\partial t}\operatorname{div} \boldsymbol{E} = 4\pi\frac{\partial \rho}{\partial t}, \quad \frac{\partial}{\partial t}\operatorname{div} \boldsymbol{H} = 4\pi\frac{\partial \rho^M}{\partial t}. \tag{12}$$

Integrating (12) with zero initial conditions, we arrive at the Gauss laws for electricity and magnetism:

$$\operatorname{div} \boldsymbol{E}(t) = 4\pi\rho(t) \quad \text{and} \quad \operatorname{div} \boldsymbol{H}(t) = 4\pi\rho^M(t). \tag{13}$$

With the help of (13), equations (9)–(10) can be reduced to the independent wave (d'Alembert) equations for $\boldsymbol{E}$ and $\boldsymbol{H}$:

$$\frac{1}{c^2}\frac{\partial^2 \boldsymbol{E}}{\partial t^2} - \Delta \boldsymbol{E} = -4\pi\left[\frac{1}{c^2}\frac{\partial \boldsymbol{j}}{\partial t} + \frac{1}{c}\operatorname{curl} \boldsymbol{j}^M + \operatorname{grad}\rho\right], \tag{14}$$

$$\frac{1}{c^2}\frac{\partial^2 \boldsymbol{H}}{\partial t^2} - \Delta \boldsymbol{H} = -4\pi \left[\frac{1}{c^2}\frac{\partial \boldsymbol{j}^M}{\partial t} - \frac{1}{c}\operatorname{curl} \boldsymbol{j} + \operatorname{grad} \rho^M \right]. \tag{15}$$

Similarly to the case of the wave equation and classical lacunae, we assume that the currents in (9)–(10) are compactly supported on a bounded space–time domain $Q = S \times [0, T_0] \subset \mathbb{R}^3 \times [0, \infty)$, i.e., they are localized in space (on the domain $S \subset \mathbb{R}^3$) and operate only for a finite interval of time T_0. Under this assumption we will show that the solutions to (14) and (15) have the so-called quasi-lacunae (see [19] for detail) that can be thought of as counterparts of classical lacunae that characterize the Maxwell system. A quasi-lacuna is the region of space–time behind the sharp aft fronts of the propagating waves where the field $\boldsymbol{E}$ or $\boldsymbol{H}$ has already reached the steady state and no longer evolves in time. The analysis of quasi-lacunae can be performed using either of the equations (14) or (15) since they have identical form. We choose equation (14) for the electric field and comment on its magnetic counterpart (15) when necessary.

In the Cartesian coordinates, equation (14) gets split into three independent 3D wave equations of type (1) for the Cartesian components E_x, E_y and E_z. We denote any of these components by $u(\boldsymbol{x}, t)$ and continue the analysis of the resulting inhomogeneous scalar wave equation. The right-hand side $f(\boldsymbol{x}, t)$ in (1) takes the form

$$f(\boldsymbol{x}, t) = -4\pi \left[\frac{1}{c^2}\frac{\partial j_i}{\partial t} + \frac{1}{c}\operatorname{curl}_i \boldsymbol{j}^M + \operatorname{grad}_i \rho \right], \tag{16}$$

where the subscript i that can be x, y, or z denotes the projection of a given vector on the corresponding Cartesian axis.

Next, as $\boldsymbol{j}(\boldsymbol{x}, t) = \boldsymbol{j}^M(\boldsymbol{x}, t) = 0$ for $t > T_0$ we can represent the right-hand side (16) as a sum of two terms:

$$f(\boldsymbol{x}, t) = f^{(1)}(\boldsymbol{x}, t)\theta(T_0 - t) + f^{(2)}(\boldsymbol{x})\theta(t - T_0), \quad \boldsymbol{x} \in S, \tag{17}$$

where

$$f^{(1)}(\boldsymbol{x}, t) = -4\pi \left[\frac{1}{c^2}\frac{\partial j_i}{\partial t} + \frac{1}{c}\operatorname{curl}_i \boldsymbol{j}^M + \operatorname{grad}_i \rho \right], \tag{18}$$

$$f^{(2)}(\boldsymbol{x}) = -4\pi \operatorname{grad}_i \rho, \tag{19}$$

and $\theta(\cdot)$ is the Heaviside function. The function (18) depends on time because the currents $\boldsymbol{j}$ and $\boldsymbol{j}^M$, generally speaking, depend on time (they operate from $t = 0$ to $t = T_0$). In addition, according to the first continuity equation in (11) the electric charge density ρ is given by

$$\rho(\boldsymbol{x}, t) = \begin{cases} -\displaystyle\int_0^t \operatorname{div} \boldsymbol{j}(\boldsymbol{x}, t')dt', & t \leqslant T_0, \\ \qquad\qquad\qquad\qquad\quad \boldsymbol{x} \in S, \\ -\displaystyle\int_0^{T_0} \operatorname{div} \boldsymbol{j}(\boldsymbol{x}, t')dt', & t > T_0, \end{cases} \tag{20}$$

which implies that for $t \leqslant T_0$ the $\operatorname{grad}_i \rho$ term in (18) also varies in time. On the contrary, the function (19) is time-independent because the second line of (20) implies that $\rho(\boldsymbol{x}, t) \equiv \rho(\boldsymbol{x})$ for all $t > T_0$.

By linearity, partition (17) implies that the overall solution can be represented as the sum:

$$u(\boldsymbol{x}, t) = u^{(1)}(\boldsymbol{x}, t) + u^{(2)}(\boldsymbol{x}, t). \tag{21}$$

The first term in this sum is given by

$$\begin{aligned} u^{(1)}(\boldsymbol{x}, t) &= \frac{1}{4\pi} \iiint\limits_{|\boldsymbol{x}-\boldsymbol{\xi}| \leq ct} \frac{\theta(T_0 - t + |\boldsymbol{x}-\boldsymbol{\xi}|/c) f^{(1)}(\boldsymbol{\xi}, t - |\boldsymbol{x}-\boldsymbol{\xi}|/c)}{|\boldsymbol{x}-\boldsymbol{\xi}|} d\boldsymbol{\xi} \\ &= \frac{1}{4\pi} \iiint\limits_{c(t-T_0) \leq |\boldsymbol{x}-\boldsymbol{\xi}| \leq ct} \frac{f^{(1)}(\boldsymbol{\xi}, t - |\boldsymbol{x}-\boldsymbol{\xi}|/c)}{|\boldsymbol{x}-\boldsymbol{\xi}|} d\boldsymbol{\xi}. \end{aligned} \tag{22}$$

Comparing (22) with (3) and keeping in mind that $f^{(1)}$ is compactly supported in space on the domain S we conclude that this component of the solution has classical primary and secondary lacunae, i.e., it is equal to zero ahead of the propagating forward front and behind the aft front of the waves. The area between these two sharp fronts contains the outgoing waves.

Next, let us consider the second term in the sum (21):

$$u^{(2)}(\boldsymbol{x}, t) = \frac{1}{4\pi} \iiint\limits_{|\boldsymbol{x}-\boldsymbol{\xi}| \leq ct} \frac{\theta(t - |\boldsymbol{x}-\boldsymbol{\xi}|/c - T_0) f^{(2)}(\boldsymbol{\xi})}{|\boldsymbol{x}-\boldsymbol{\xi}|} d\boldsymbol{\xi} = \frac{1}{4\pi} \iiint\limits_{|\boldsymbol{x}-\boldsymbol{\xi}| \leq c(t-T_0)} \frac{f^{(2)}(\boldsymbol{\xi})}{|\boldsymbol{x}-\boldsymbol{\xi}|} d\boldsymbol{\xi}. \tag{23}$$

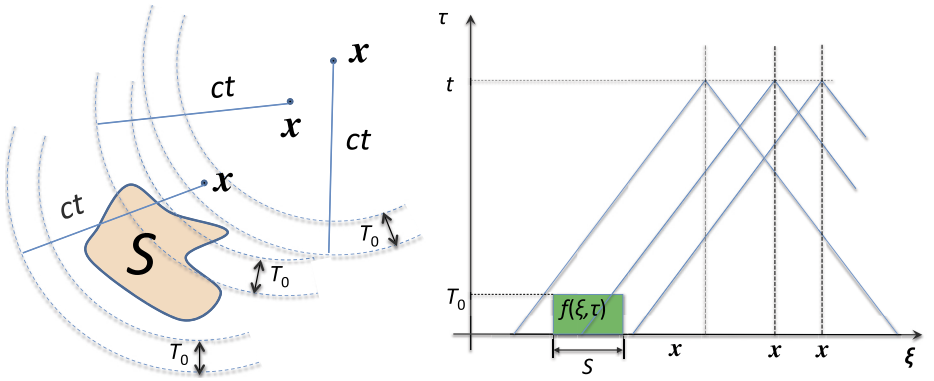

Fig. 2. The integration area in (23) for different $\boldsymbol{x}$ at a fixed t and its overlap with the support S of $f^{(2)}$.

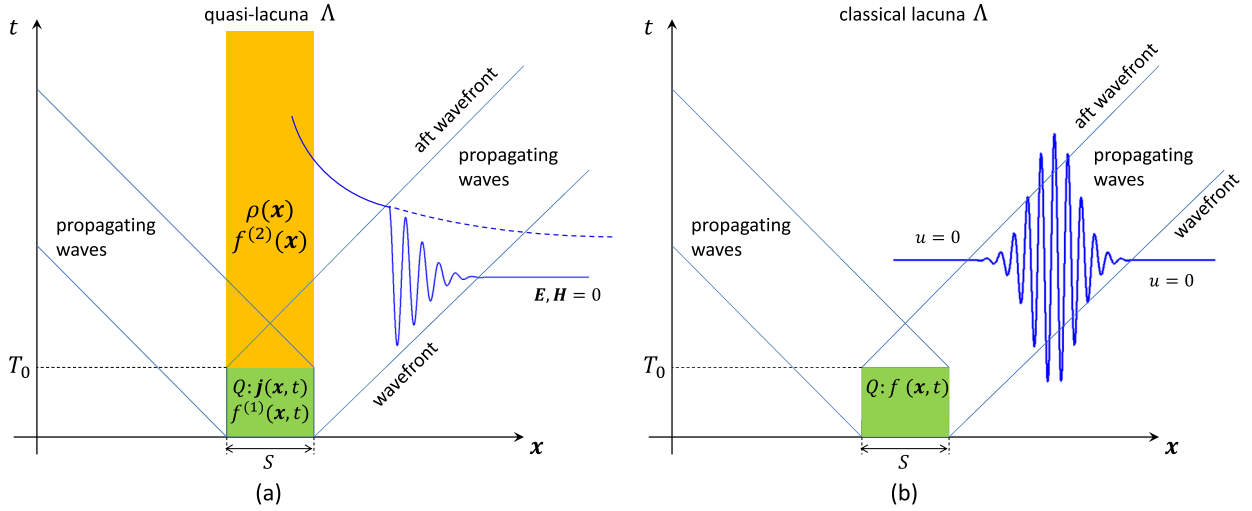

Fig. 3. (a) Quasi-lacuna of Maxwell's equations and (b) classical lacuna of the 3D wave equation driven by compactly supported sources (green areas). In the case (a), the charge density $\rho(\boldsymbol{x})$ accumulated by the time $t = T_0$ generates a steady-state solution that occupies the quasi-lacuna. The blue curve in both panels, (a) and (b), schematically represents the spatial profile of the overall solution at a fixed t. The dotted continuation into the zone of propagating waves and beyond shown in (a) is the genuine steady-state field generated by $\rho(\boldsymbol{x})$ (as $t \to \infty$). (For interpretation of the references to color in this figure legend, the reader is referred to the web version of this article.)

We would like to analyze the solution $u^{(2)}$ given by (23) inside the secondary lacuna Λ of (8). Suppose that $(\boldsymbol{x}, t) \in \Lambda$, i.e., that at a given t the point $\boldsymbol{x}$ belongs to the domain Λ_1 of (6). This means that the entire spatial support S of $f^{(2)}$ lies inside the integration ball of radius $c(t - T_0)$ centered at $\boldsymbol{x}$. Therefore, we can reduce the integration area in (23) to S, which yields:

$$u^{(2)}(\boldsymbol{x}, t) = \frac{1}{4\pi} \iiint\limits_S \frac{f^{(2)}(\boldsymbol{\xi})}{|\boldsymbol{x} - \boldsymbol{\xi}|} d\boldsymbol{\xi}, \quad (\boldsymbol{x}, t) \in \Lambda. \tag{24}$$

Formula (24) shows that the solution inside the lacuna can be represented as the Coulomb potential due to compactly supported density $f^{(2)}(\boldsymbol{\xi})$. The function $u^{(2)}(\boldsymbol{x}, t)$ is obviously an electrostatic solution and satisfies the Poisson equation $\Delta u^{(2)} = -f^{(2)}$. The key difference between $u^{(2)}(\boldsymbol{x}, t)$ of (24) and the true Coulomb potential is that representation (24) holds only inside the lacuna Λ.

To demonstrate that, let us fix the moment of time t and choose $\boldsymbol{x}$ outside Λ_1, i.e., further away from S than allowed by (6). In this case, the overlap between the integration area in (23) and the support S of $f^{(2)}$ will first be shrinking as $\boldsymbol{x}$ moves away from S, see Fig. 2. This will lead to a variation of the solution $u^{(2)}(\boldsymbol{x}, t)$. For the points $\boldsymbol{x}$ that are sufficiently far from S, specifically, $\mathrm{dist}(\boldsymbol{x}, S) > c(t - T_0)$, the intersection between the integration area and S becomes empty. This implies $u^{(2)}(\boldsymbol{x}, t) = 0$. The locus of all $\boldsymbol{x}$ that correspond to the shrinking overlap between the integration area and S is the region where the outgoing waves are at the current moment of time t. The locus of all $\boldsymbol{x}$ for which the aforementioned intersection is empty is the region exterior to the propagating forward front (i.e., the spatial cross-section Λ_0 of the primary lacuna).

Thus, the structure of the overall solution (21) is as follows, see Fig. 3(a). Behind the aft front $u^{(1)}(\boldsymbol{x}, t) = 0$ and $u^{(2)}(\boldsymbol{x}, t)$ is given by the Coulomb potential (24). At the aft front, the Coulomb electrostatic solution matches the unsteady outgoing

waves given by the sum of $u^{(1)}(\boldsymbol{x},t)$ of (22) and $u^{(2)}(\boldsymbol{x},t)$ of (23). In turn, the outgoing waves that occupy the region between the secondary lacuna and the primary lacuna die off at the forward propagating wavefront due to the causality. For the purpose of comparison, in Fig. 3(b) we are showing a schematic of the corresponding solution to the plain wave equation. The main difference between Figs. 3(a) and 3(b) is in how the solution behaves behind the aft front, i.e., in the area of the secondary lacuna. In the classical case of the wave equation it is zero, whereas in the case of Maxwell's equations this solution does not depend on time, yet generally speaking it is non-zero. Therefore, in our work [19] we introduced a special new term *quasi-lacuna* to describe the region behind the aft fronts of the waves for Maxwell's equations. In the case of electromagnetic fields and accumulated charges, it replaces the notion of classical lacunae. As the time elapses, the quasi-lacuna in the solution of Maxwell's equations expands, see Fig. 3(a), and accordingly, the electrostatic solution (24) occupies a larger part of space. As $t\to\infty$, a full transition to steady state occurs and the electrostatic solution (24) becomes a genuine Coulomb potential over the entire $\mathbb{R}^3$ (the dotted blue line in Fig. 3(a)).

The foregoing results can be summarized in a theorem that we reproduce from our work [19] and formulate in terms of electromagnetic fields:

Theorem 1. *Let the electric and magnetic fields $\boldsymbol{E}=\boldsymbol{E}(\boldsymbol{x},t)$ and $\boldsymbol{H}=\boldsymbol{H}(\boldsymbol{x},t)$, $\boldsymbol{x}\in\mathbb{R}^3$, $t\geq 0$, be governed by Maxwell's equations (9)–(10) subject to zero initial conditions. Let the electric $\boldsymbol{j}=\boldsymbol{j}(\boldsymbol{x},t)$ and the magnetic $\boldsymbol{j}^M=\boldsymbol{j}^M(\boldsymbol{x},t)$ current densities be compactly supported in space–time on the region $Q=S\times[0,T_0]$, and let the electric and magnetic charge densities $\rho=\rho(\boldsymbol{x},t)$ and $\rho^M=\rho^M(\boldsymbol{x},t)$ be equal to zero at $t=0$ for all $\boldsymbol{x}\in\mathbb{R}^3$. Then, the solution for the fields $\boldsymbol{E}$ and $\boldsymbol{H}$ on the region of space–time Λ defined by formula (8) satisfies the electrostatic equations in space:*

$$\Delta\boldsymbol{E}=4\pi\,\mathrm{grad}\rho, \tag{25}$$

$$\Delta\boldsymbol{H}=4\pi\,\mathrm{grad}\rho^M, \tag{26}$$

for every moment of time t. The right-hand sides of equations (25) and (26) are defined via the gradients of the densities of the electric and magnetic charge accumulated during the operational period of the respective currents:

$$\rho(\boldsymbol{x})=-\int_0^{T_0}\mathrm{div}\,\boldsymbol{j}(\boldsymbol{x},t')dt',\quad \rho^M(\boldsymbol{x})=-\int_0^{T_0}\mathrm{div}\,\boldsymbol{j}^M(\boldsymbol{x},t')dt'.$$

For a given t, the electric and magnetic fields on the bounded domain $\Lambda_1=\{\Lambda\cap\{t=\mathrm{const}\}\}\subset\mathbb{R}^3$, see formula (6), are obtained by truncating the solutions $\boldsymbol{E}$ and $\boldsymbol{H}$ to the Poisson equations (25) and (26), respectively, that vanish at infinity if considered on the entire $\mathbb{R}^3$.

Theorem 1 shows that the Huygens' principle for Maxwell's equations in 3D holds, i.e., that the solutions to these equations exhibit sharp aft fronts. The key difference compared to the scalar wave equation is that for Maxwell's equations the residual solution behind the aft fronts is, generally speaking, not zero. In other words, the classical lacunae are replaced with quasi-lacunae.

In real physical settings, solutions to Maxwell's equations (9)–(10) make sense only if the magnetic current is zero (as no magnetic charges exist). Then, the region Λ of (8) becomes a classical lacuna for the magnetic field, i.e., $\boldsymbol{H}(\boldsymbol{x},t)=0$ if $(\boldsymbol{x},t)\in\Lambda$. Otherwise, a sufficient condition for the quasi-lacuna for either electric or magnetic field to become classical is that the corresponding current must be solenoidal, i.e., $\mathrm{div}\,\boldsymbol{j}=0$ or $\mathrm{div}\,\boldsymbol{j}^M=0$ for all $t<T_0$.

Note also that equations (25) and (26) allow for the representation of $\boldsymbol{E}$ and $\boldsymbol{H}$ via the respective potentials:

$$\boldsymbol{E}=-\mathrm{grad}\varphi,$$

$$\boldsymbol{H}=-\mathrm{grad}\varphi^M,$$

where

$$\Delta\varphi=-4\pi\rho\quad\text{and}\quad\Delta\varphi^M=-4\pi\rho^M.$$

4. Lacunae-based time marching for Maxwell's equations

In this section, we outline the idea of how to use the quasi-lacunae for solving Maxwell's equations in vacuum on bounded domains. Later, it will be incorporated into a more general algorithm for solving the non-Huygens' problems that have neither classical lacunae nor quasi-lacunae.

Suppose we need to solve the Maxwell system (9)–(10) on a bounded computational domain S. First, we will assume that the currents $\boldsymbol{j}$ and $\boldsymbol{j}_M$ are compactly supported on S and operate during a finite interval $[t_0,t_1]$. Due to the existence of quasi-lacunae, by the time $t_2=t_0+T_{\mathrm{int}}$, where

$$T_{\mathrm{int}}\equiv\frac{1}{c}\mathrm{diam}\,S+T_0\quad\text{and}\quad T_0\equiv t_1-t_0, \tag{27}$$

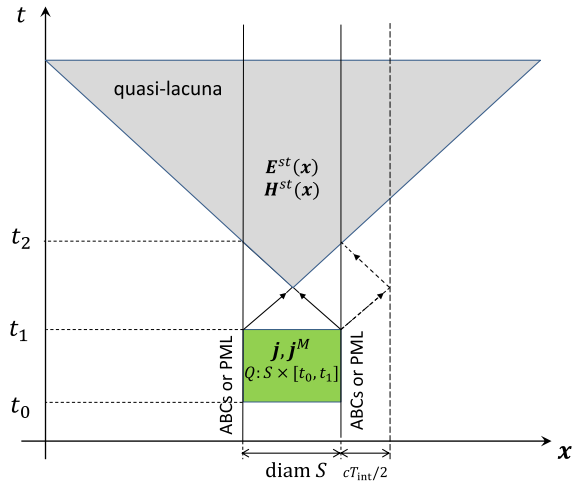

Fig. 4. Quasi-lacuna of Maxwell's equations (gray-shaded area) generated by compactly supported currents (green area). Two possible options of handling the artificial boundaries include (i) setting an ABC/PML at ∂S that would provide sufficient accuracy and stability within the integration interval $[t_0, t_2]$ or (ii) placing the outer boundaries at the distance $cT_{\text{int}}/2$ from the domain of interest S so that the reflected waves will not reach S before t_2. (For interpretation of the references to color in this figure legend, the reader is referred to the web version of this article.)

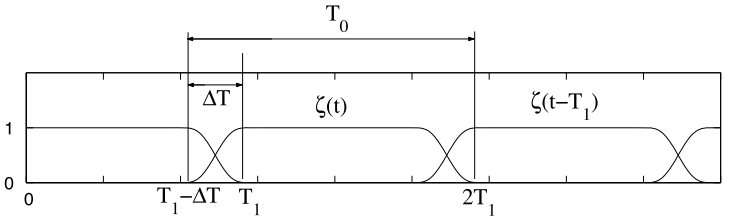

Fig. 5. Partition of unity for the time variable.

the solution on the computational domain S will no longer be evolving in time, see Fig. 4. Hence, we need to compute this solution only over the finite time interval T_{int} given by (27). It is therefore sufficient to place an artificial outer boundary far enough from the domain of interest S so that the reflected waves will not reenter S before we terminate the computation. Specifically, the outer boundary should be placed no closer than the distance $cT_{\text{int}}/2$ from ∂S. Then, the solution of Maxwell's equations inside S during the time interval T_{int} will not be affected by this outer boundary at all. In other words, it will be exactly the same as if the Maxwell equations were solved on the entire $\mathbb{R}^3$. In this sense, the use of quasi-lacunae eliminates the need for a special treatment of artificial outer boundaries yet still allows one to compute the solution only on a bounded domain, which is feasible from the standpoint of practice.

As an alternative to placing the outer boundary at a distance from ∂S, we can set an ABC or a PML right at ∂S, see Fig. 4. This approach does not require solving the Maxwell equations in the region of the width $cT_{\text{int}}/2$ exterior to ∂S, which reduces the cost. At the same time, it puts a less stringent requirement on the performance of the chosen ABC or PML. Indeed, due to the quasi-lacuna the ABC no longer has to maintain its desired non-reflecting properties indefinitely. It only needs to do so for the duration of the required integration interval $T_{\text{int}} = t_2 - t_0$ of (27).

Next, consider a more general case where the currents $\boldsymbol{j}$ and $\boldsymbol{j}^M$ operate continuously in time yet remain compactly supported in space on S. As shown in Fig. 5, introduce a smooth partition of unity:

$$\begin{aligned} &\forall t \geqslant 0: \quad 1 = \sum_{i=0}^{\infty} \zeta\,(t - (i-1)T_1), \\ &T_1 = T_0 - \Delta T, \quad \text{and} \quad \operatorname{supp} \zeta(t) = [T_1 - \Delta T, 2T_1], \end{aligned} \tag{28}$$

where T_0 is the size of each partition element and ΔT is the width of the overlapping interval. By $\zeta(t)$ we denote a smooth compactly supported function such that $\zeta(1) = 1$ for $T_1 \leqslant t \leqslant 2T_1 - \Delta T$ and $\zeta(t) + \zeta(t + T_1) = 1$ for $T_1 - \Delta T \leqslant t \leqslant T_1$. All of the partition elements can be obtained from one another by a simple translation $t \mapsto t + (i-1)T_1$, $i = 0, 1, \ldots$[3]

[3] Note that the interval ΔT over which the function $\zeta(t)$ increases from 0 and 1 cannot be chosen too short. Indeed, a very sharp transition from 0 to 1 may look like a discontinuity on the grid. Then, the quality of the discrete solution will deteriorate and the lacunae will get contaminated by numerical artifacts. In practice, we chose ΔT 15 to 20 times larger than the time step τ of the discretization scheme, see Section 8.3.

Multiplying the current densities $\boldsymbol{j}$ and $\boldsymbol{j}^M$ by the sum given in formula (28), we transform these continuously operating currents into the sums of partial sources that operate only during a fixed finite time interval each:

$$\begin{aligned} \boldsymbol{j}(\boldsymbol{x},t) &= \sum_{i=0}^{\infty} \boldsymbol{j}_i(\boldsymbol{x},t), \quad \boldsymbol{j}_i(\boldsymbol{x},t) = \boldsymbol{j}(\boldsymbol{x},t)\zeta\left(t-(i-1)T_1\right), \\ \boldsymbol{j}^M(\boldsymbol{x},t) &= \sum_{i=0}^{\infty} \boldsymbol{j}_i^M(\boldsymbol{x},t), \quad \boldsymbol{j}_i^M(\boldsymbol{x},t) = \boldsymbol{j}^M(\boldsymbol{x},t)\zeta\left(t-(i-1)T_1\right). \end{aligned} \tag{29}$$

An individual i-th partial current is turned on at the moment

$$t_0^{(i)} = \begin{cases} 0, & i=0, \\ iT_1 - \Delta T, & i=1,2,\ldots \end{cases} \tag{30}$$

and is turned off at

$$t_1^{(i)} = (i+1)T_1. \tag{31}$$

Thus, it operates for exactly T_0 "seconds."

By linear superposition, the original system (9)–(10) can now be decomposed into a series of independent partial subsystems (indexed by $i=0,1,2,\ldots$) driven by the partial currents (29). The solutions to these partial subsystems are turned on at the moments $t_0^{(i)}$ since their respective sources are zero prior to that, and the initial conditions are also homogeneous. Those solutions have quasi-lacunae, i.e., they reach their respective (non-zero) steady states on S at $t_2^{(i)} = t_0^{(i)} + T_{\text{int}}$, where T_{int} is given by (27). As such, each of these subsystems can be solved on the domain S as described in the beginning of the section, i.e., either by placing an artificial outer boundary at the distance $cT_{\text{int}}/2$ from ∂S or by setting an ABC/PML at ∂S. In the first case, the lacunae-based algorithm essentially eliminates the need for a special treatment of the artificial outer boundary yet keeps the computational domain bounded for all times. In the second case, as long as the chosen ABC or PML appears sufficiently accurate and stable over the interval T_{int}, the lacunae-based algorithm extends this behavior to arbitrarily long time intervals.

Indeed, according to the partition (29), at any moment of time the overall solution to (9)–(10) can be represented as

$$\boldsymbol{E}(\boldsymbol{x},t) = \sum_{i=0}^{N_0-1} \boldsymbol{E}_i^{\text{st}}(\boldsymbol{x},t) + \sum_{i=N_0}^{N_1} \boldsymbol{E}_i(\boldsymbol{x},t) \tag{32}$$

$$\boldsymbol{H}(\boldsymbol{x},t) = \sum_{i=0}^{N_0-1} \boldsymbol{H}_i^{\text{st}}(\boldsymbol{x},t) + \sum_{i=N_0}^{N_1} \boldsymbol{H}_i(\boldsymbol{x},t). \tag{33}$$

The fields given by the right-hand sides of (32) and (33) are split into two sums according to the nature of the terms in these sums. The terms in the first sum in each of the formulae (32) and (33) represent the residual steady-state fields of the "mature" partial subproblems, i.e., those problems for which their quasi-lacuna already contains the entire domain S.

The second sum in (32) or (33) is composed of the unsteady solutions to the relatively recent subproblems with the quasi-lacuna that has not covered the entire S yet. The first such problem corresponds to the lower summation limit $N_0 = \left\lfloor \frac{t-\operatorname{diam} S/c}{T_0} \right\rfloor$. The upper limit $N_1 = \lceil t/T_0 \rceil - 1$ of the second sum in each of the formulae (32) and (33) is finite due to the causality, because the solutions to the "future" problems, i.e., the problems with the sources that have not started to operate yet at the time t, are zero. Here we denote by $\lceil\cdot\rceil$ the ceiling function, i.e., the function that yields the nearest integer greater or equal to its argument. It is very important that the number of terms in the second sum is finite and bounded for any t, namely $N_1 - N_0 + 1 \leqslant \left\lceil \frac{\operatorname{diam} S/c}{T_0} \right\rceil + 2$.

In the case of classical lacunae the steady-state terms that compose the first sum in either (32) or (33) are all equal to zero. The second sum has a finite non-increasing number of terms, and each of these terms needs to be computed only for a finite non-increasing time interval T_{int}. This allowed us to prove a temporally uniform error bound for the solutions represented by means of (32) and (33), see [23]. Such an estimate implies, in particular, that even if the performance of the chosen ABC or PML deteriorates for longer times, i.e., those beyond T_{int}, the solution computed with the help of the lacunae-based algorithm will not be subject to a similar deterioration.

In the case of quasi-lacunae, the steady-state components of the fields in the first sum of either (32) or (33) are non-zero and may accumulate over time since N_0 increases as t increases. Yet if the current densities $\boldsymbol{j}$ and $\boldsymbol{j}^M$ are given, then one does not need to compute the individual contributions $\boldsymbol{E}_i^{\text{st}}(\boldsymbol{x},t)$ and $\boldsymbol{H}_i^{\text{st}}(\boldsymbol{x},t)$ for each $i=0,1,2,\ldots$. Instead, one can compute the overall steady-state contribution only once for the final moment of time. This allowed us to extend the aforementioned temporally uniform error bound to the case of quasi-lacunae as well, see [23].

However, our ultimate goal is to apply the lacunae-based algorithm to non-Huygens' problems that may have a complex formulation in the near field while reducing to the pure Maxwell equations in the far field. As shown in Section 5, in this

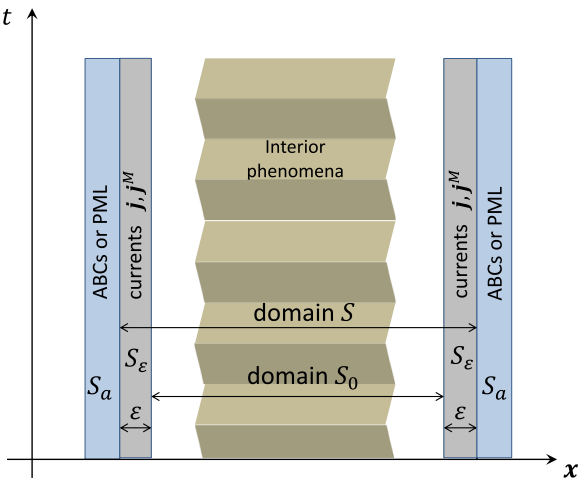

Fig. 6. Decomposition of the original non-Huygens' problem into the interior and auxiliary problems.

case the currents $\boldsymbol{j}$ and $\boldsymbol{j}^M$ are not given ahead of time; they are rather determined in the course of time marching. Then, one needs to compute numerically all individual non-zero steady-state components $\boldsymbol{E}_i^{\mathrm{st}}(\boldsymbol{x},t)$ and $\boldsymbol{H}_i^{\mathrm{st}}(\boldsymbol{x},t)$ in (32) and (33). This may potentially cause the growth of the error in time, because the number of terms in the first sum in either (32) or (33) increases as the time elapses. The main result of the current paper is that we modify the partial subproblems for Maxwell's equations so as to provably prevent any possible error growth due to the accumulating steady-state components of the solution.

5. Non-Huygens' problems and the decomposition technique

Let us consider the following problem on the entire $\mathbb{R}^3$:

$$\hat{\mathbf{F}}\left(\boldsymbol{x},t,\boldsymbol{w},\frac{\partial \boldsymbol{w}}{\partial t},\frac{\partial \boldsymbol{w}}{\partial \boldsymbol{x}},\dots\right)=\mathbf{0},\quad \boldsymbol{x}\in S_0,\ t>0, \tag{34}$$

$$\frac{1}{c}\frac{\partial \boldsymbol{w}}{\partial t}+\hat{\mathbf{L}}\boldsymbol{w}=\mathbf{0},\quad \boldsymbol{x}\in\mathbb{R}^3\backslash S_0,\ t>0, \tag{35}$$

$$\boldsymbol{w}(\boldsymbol{x},0)=\mathbf{0},\quad \boldsymbol{x}\in\mathbb{R}^3\backslash S_0. \tag{36}$$

In formulae (34)–(36), $S_0\subset\mathbb{R}^3$ is a bounded domain in space, $\boldsymbol{w}(\boldsymbol{x},t)=[\boldsymbol{E},\boldsymbol{H}]^T$ is the vector of field components, and

$$\hat{\mathbf{L}}=\begin{bmatrix}0 & -\operatorname{curl}\\ \operatorname{curl} & 0\end{bmatrix}$$

is a differential operator acting on $\boldsymbol{w}$.

In formula (34), $\hat{\mathbf{F}}(\cdots)$ denotes an abstract operator that defines the governing equations for the complex electromagnetic phenomena that may take place in the near field, i.e., on the domain S_0 (e.g., propagation, scattering, absorption, interaction with non-linear media, etc.). We impose no constraints on these equations except for the following two: (i) we assume that outside S_0 equations (34) smoothly transition (no discontinuities in the coefficients, etc.) into equations (35), i.e., into the homogeneous Maxwell equations in vacuum and (ii) the overall problem (34)–(36) is well-posed (which, in particular, means uniquely solvable).

Problem (34)–(36) is formulated on $\mathbb{R}^3$. In practice, however, we have to solve this problem numerically on a bounded domain. A natural choice for this domain would be S_0 itself where the most interesting physics takes place. However, for future convenience we rather surround S_0 with an additional layer of width ε. In other words, we choose the computational domain $S=S_0\cup S_\varepsilon$, where $S_\varepsilon=\{\boldsymbol{x}|\boldsymbol{x}\in\mathbb{R}^3\backslash S_0,\ \operatorname{dist}(\boldsymbol{x},\partial S_0)<\varepsilon\}$, see Fig. 6. The computational domain S needs to be terminated by an ABC or a PML at the outer boundary ∂S. In the numerical context, the PML S_a is a layer of finite thickness that surrounds the computation domain, see Fig. 6. Inside this layer, the governing equations are modified so as to render the absorption of the outgoing waves. An ABC in practice can be set directly at the outer boundary ∂S. We require that the chosen ABC or PML be sufficiently accurate and stable at least for moderate times that can still be much shorter than the overall desired duration of simulation.

As problem (34) on S_0 is almost arbitrary and, generally speaking, non-Huygens, we cannot use directly the quasi-lacunae approach from Section 4, because it is valid only for Maxwell's equations in vacuum. Therefore we decompose the overall

problem (34)–(36) into the interior problem (IP) and auxiliary problem (AP). The interior problem has the form:

$$\begin{aligned}
&\hat{\mathbf{F}}\left(\boldsymbol{x}, t, \boldsymbol{w}, \frac{\partial \boldsymbol{w}}{\partial t}, \frac{\partial \boldsymbol{w}}{\partial \boldsymbol{x}}, \dots\right) = \mathbf{0}, \quad \boldsymbol{x} \in S_0,\ t > 0, \\
&\frac{1}{c}\frac{\partial \boldsymbol{w}}{\partial t} + \hat{\mathbf{L}}\boldsymbol{w} = \mathbf{0}, \quad \boldsymbol{x} \in S_\varepsilon,\ t > 0, \\
&\boldsymbol{w}(\boldsymbol{x}, t) = \boldsymbol{w}^{\text{aux}}(\boldsymbol{x}, t), \quad \boldsymbol{x} \in \Gamma,\ t > 0.
\end{aligned} \tag{37}$$

where $\Gamma = \partial S$ is the boundary of the computational domain. Problem (37) includes equations (34) on S_0 that smoothly transition to the pure Maxwell equations on S_ε. At the outer boundary Γ, the IP (37) is terminated by the boundary conditions provided by the auxiliary problem.

The auxiliary problem is the pure Maxwell system considered on the entire space:

$$\begin{aligned}
&\frac{1}{c}\frac{\partial \boldsymbol{w}^{\text{aux}}}{\partial t} + \hat{\mathbf{L}}\boldsymbol{w}^{\text{aux}} = \boldsymbol{f}^{\text{aux}}(\boldsymbol{x}, t), \quad \boldsymbol{x} \in \mathbb{R}^3,\ t > 0, \\
&\boldsymbol{w}^{\text{aux}}(\boldsymbol{x}, 0) = \mathbf{0}, \quad \boldsymbol{x} \in \mathbb{R}^3,
\end{aligned} \tag{38}$$

and driven by the auxiliary currents $\boldsymbol{f}^{\text{aux}}(\boldsymbol{x}, t) = -\frac{4\pi}{c}\left[\boldsymbol{j}, \boldsymbol{j}^{\text{M}}\right]^T$ of a special kind. Those currents are constructed as follows.

First, we introduce a smooth function $\mu(\boldsymbol{x})$, $\boldsymbol{x} \in \mathbb{R}^3$, such that $\mu(\boldsymbol{x}) = 0$ for $\boldsymbol{x} \in S_0$, i.e., inside S_0, and $\mu(\boldsymbol{x}) = 1$ for $x \in \mathbb{R}^3 \backslash S$, i.e., outside the computational domain S. In the near-boundary layer S_ε, this function increases smoothly from zero to one. Qualitatively, the profile of this function in the direction of its growth resembles a smoothed step (Heaviside) function. For this reason, we will sometimes refer to the function μ as to a "smoothed step function."

Next, suppose we know the solution $\boldsymbol{w}(\boldsymbol{x}, t) = [\boldsymbol{E}, \boldsymbol{H}]^T$ to problem (34)–(36) on the entire space and for all $t \geqslant 0$. We multiply $\boldsymbol{w}(\boldsymbol{x}, t)$ by the scalar function $\mu(\boldsymbol{x})$ and apply the differential operator of the pure Maxwell system to the resulting product on $\mathbb{R}^3 \times [0, +\infty)$:

$$\boldsymbol{f}^{\text{aux}}(\boldsymbol{x}, t) \stackrel{\text{def}}{=} \frac{1}{c}\frac{\partial \mu \boldsymbol{w}}{\partial t} + \hat{\mathbf{L}}\mu\boldsymbol{w}, \tag{39}$$

or, in the component form,

$$\boldsymbol{j} = -\frac{c}{4\pi}\left[\frac{1}{c}\frac{\partial \mu \boldsymbol{E}}{\partial t} - \operatorname{curl} \mu \boldsymbol{H}\right], \tag{40}$$

$$\boldsymbol{j}^M = -\frac{c}{4\pi}\left[\frac{1}{c}\frac{\partial \mu \boldsymbol{H}}{\partial t} + \operatorname{curl} \mu \boldsymbol{E}\right]. \tag{41}$$

Clearly, the quantities (39)–(41) are identically equal to zero on S_0 because $\mu(\boldsymbol{x}) = 0$ there. On the other hand, those quantities also turn into zero outside the computational domain, i.e., on $\mathbb{R}^3 \backslash S$, because the function $\mu(\boldsymbol{x})$ is equal to one there and, according to (35), the solution $\boldsymbol{w}(\boldsymbol{x}, t) = [\boldsymbol{E}, \boldsymbol{H}]^T$ satisfies the pure Maxwell system already outside S_0 and, hence, outside S. Consequently, we conclude that: (i) the currents built this way differ from zero only in the near-boundary layer S_ε and, more importantly, (ii) to construct these currents, we need to know the solution $\boldsymbol{w}(\boldsymbol{x}, t)$ to the original problem (34)–(36) only on S_ε, i.e., near the boundary of the computational domain. In practice, it means that in order to generate the sources for the AP we can use the solution to the interior problem (37) rather than to the overall problem (34)–(36).

Furthermore, substituting the source function (39) into the right-hand side of the AP (38) one obviously obtains that $\boldsymbol{w}^{\text{aux}} \equiv \mu \boldsymbol{w}$ since the pure Maxwell system is uniquely solvable. Therefore, at the boundary of the computational domain Γ where $\mu = 1$ we have $\boldsymbol{w}^{\text{aux}} = \boldsymbol{w}$ and consequently, the solution to the AP on Γ can indeed provide the boundary data for the IP, see (37).

Hence, the IP (37) and the AP (38) are intertwined with each other as follows: the solution to the IP (which is, of course, of primary interest on its own) is used for constructing the currents for the AP. The latter, in turn, provides the boundary closure for the IP. Note that the AP is still posed on the entire $\mathbb{R}^3$ and in practice it has to be truncated by means of an ABC or a PML.

As $\boldsymbol{w}^{\text{aux}} \equiv \mu \boldsymbol{w}$ and $\mu = 0$ on S_0, one may suggest to solve the AP (38) only on $\mathbb{R}^3 \backslash S_0$ (or, in the numerical context, on $S_\epsilon \cup S_a$). However, $\boldsymbol{w}^{\text{aux}}$ is subject to further partitioning in time, i.e., to decomposition into the sums (32)–(33). While the overall sums (32)–(33) are equal zero on $\mathbb{R}^3 \backslash S_0$, their individual terms, generally speaking, are not. Therefore, each partial solution $\boldsymbol{w}_i^{\text{aux}}$ has to be computed on the entire $\mathbb{R}^3$ (truncated by an ABC/PML in practice).

A key advantage of having the original problem (34)–(36) decomposed into the IP and AP is that the AP is of the Huygens' type. Therefore, to solve it we can employ the time marching technique based on quasi-lacunae, as outlined in Section 4. In doing so, one can expect that the performance of the chosen ABC or PML will not deteriorate during long runs. Alternatively, lacunae-based time marching can be used in the capacity of a standalone closure at the artificial outer boundary. In this case, one can expect no error associated with the domain truncation.

A combined algorithm based on the decomposition of the original problem into the IP and AP and subsequent integration of the AP by means of the lacunae-based time marching was built in [23]. Its non-deteriorating performance has been

corroborated by a series of numerical simulations. As, however, explained in the remainder of this section (see, in particular, the last two paragraphs right before the beginning of Section 6), the arguments of Section 4 do not immediately apply to the combined IP/AP formulation, because the auxiliary currents (40)–(41) are not given ahead of time and are rather determined in the course of integration. Still, no accumulation of error has ever been observed in the computations of [23]. On the other hand, in the case of a combined formulation no temporally uniform error bound could be justified in [23] either.

Hereafter, we will further develop the approach of [23] and show that due to the special structure of the auxiliary currents (40)–(41) one can construct a time marching algorithm for the AP based on classical lacunae rather than quasi-lacunae. This, in turn, allows us to prove a temporally uniform error estimate for the non-Huygens' case, see Section 7.

Suppose that we know the solution $\boldsymbol{w}(\boldsymbol{x},t)$ to problem (34)–(36) on the layer S_ε at any $t\geqslant 0$. As we have shown, this is sufficient for constructing the currents (40)–(41) that drive the AP. Then, we use the partition of unity and multiply (40)–(41) by the sum on the right-hand side of (28). This yields the individual terms in the sums (29):

$$\boldsymbol{j}_i(\boldsymbol{x},t)=-\frac{c}{4\pi}\eta_i(t)\left[\frac{1}{c}\frac{\partial\mu\boldsymbol{E}}{\partial t}-\operatorname{curl}\,\mu\boldsymbol{H}\right], \tag{42}$$

$$\boldsymbol{j}_i^M(\boldsymbol{x},t)=-\frac{c}{4\pi}\eta_i(t)\left[\frac{1}{c}\frac{\partial\mu\boldsymbol{H}}{\partial t}+\operatorname{curl}\,\mu\boldsymbol{E}\right], \tag{43}$$

where we have introduced the notation $\eta_i(t)=\zeta\,(t-(i-1)T_1)$.

Now let us calculate the divergence of the partial currents (42)–(43). Since $\operatorname{div}\operatorname{curl}\equiv 0$ and $\eta_i(t)$ depends only on t we have:

$$\operatorname{div}\,\boldsymbol{j}_i(\boldsymbol{x},t)=-\frac{\eta_i(t)}{4\pi}\frac{\partial}{\partial t}\operatorname{div}\mu\boldsymbol{E}=-\frac{\eta_i(t)}{4\pi}\frac{\partial}{\partial t}\left\{\mu\operatorname{div}\boldsymbol{E}+(\operatorname{grad}\mu,\boldsymbol{E})\right\}, \tag{44}$$

$$\operatorname{div}\,\boldsymbol{j}_i^M(\boldsymbol{x},t)=-\frac{\eta_i(t)}{4\pi}\frac{\partial}{\partial t}\operatorname{div}\mu\boldsymbol{H}=-\frac{\eta_i(t)}{4\pi}\frac{\partial}{\partial t}\left\{\mu\operatorname{div}\boldsymbol{H}+(\operatorname{grad}\mu,\boldsymbol{H})\right\}, \tag{45}$$

where we have taken into account that $\operatorname{div}c\boldsymbol{a}=c\operatorname{div}\boldsymbol{a}+(\operatorname{grad}c,\boldsymbol{a})$ for a scalar c and a vector $\boldsymbol{a}$.

Recall that $\boldsymbol{E}$ and $\boldsymbol{H}$ in (44)–(45) solve the homogeneous Maxwell equations with the currents vanishing on $\mathbb{R}^3\backslash S_0$. Since the domain $\mathbb{R}^3\backslash S_0$ is free of currents, the electric and magnetic charges do not accumulate there either. They stay equal to their zero initial values for all $t\geqslant 0$, according to the continuity equations (11) with homogeneous initial conditions. In turn, the Gauss laws (13) imply that

$$\operatorname{div}\boldsymbol{E}=\operatorname{div}\boldsymbol{H}=0\quad\text{on}\quad\mathbb{R}^3\backslash S_0 \tag{46}$$

for any moment of time. This is not the case for the domain S_0 itself where the governing equations (34) may be complex and in general $\operatorname{div}\boldsymbol{E}\neq 0$ and $\operatorname{div}\boldsymbol{H}\neq 0$. However, on the domain S_0 we have $\mu\equiv 0$ by design. Altogether, we conclude that the terms $\mu\operatorname{div}\boldsymbol{E}$ and $\mu\operatorname{div}\boldsymbol{H}$ in (44)–(45) vanish everywhere on $\mathbb{R}^3$. Note also that if $\boldsymbol{H}$ is the actual physical magnetic field, then $\operatorname{div}\boldsymbol{H}\equiv 0$.

Consequently, the divergence of the currents (42)–(43) takes the form:

$$\operatorname{div}\,\boldsymbol{j}_i(\boldsymbol{x},t)=-\frac{\eta_i(t)}{4\pi}\frac{\partial}{\partial t}\operatorname{div}\mu\boldsymbol{E}=-\frac{\eta_i(t)}{4\pi}\frac{\partial}{\partial t}(\operatorname{grad}\mu,\boldsymbol{E}), \tag{47}$$

$$\operatorname{div}\,\boldsymbol{j}_i^M(\boldsymbol{x},t)=-\frac{\eta_i(t)}{4\pi}\frac{\partial}{\partial t}\operatorname{div}\mu\boldsymbol{H}=-\frac{\eta_i(t)}{4\pi}\frac{\partial}{\partial t}(\operatorname{grad}\mu,\boldsymbol{H}). \tag{48}$$

Expressions (47)–(48) differ from zero only in the near-boundary layer S_ε, where the gradient of the smoothed step function μ is non-zero. Hence, the currents (42)–(43) are, generally speaking, not solenoidal, and according to the continuity equations (11) the electric and magnetic charges may accumulate on S_ε, see Appendix A for detail. For each partial current (42)–(43), this accumulation goes on for as long as this current operates, i.e., for T_0 "seconds," and may result in a non-zero charge distribution on S_ε. We emphasize that we are talking about the currents and charges of the AP, which is a formal auxiliary construct that does not necessarily represent a physical reality. Therefore, the terms "currents" and "charges" in the context of the AP should not be understood literally, as physical quantities (especially, the non-existing in nature magnetic currents). Those terms rather represent a conventional way of describing the sources for Maxwell's equations (38). Note also that even if $\boldsymbol{H}$ is a solenoidal physical field, i.e., $\operatorname{div}\boldsymbol{H}=0$, the magnetic charge for the AP may still accumulate according to formula (48).

As shown in Section 3, the accumulated charges generate a non-zero steady-state contribution to the solution of every partial subproblem inside its quasi-lacuna. Those steady-state components cannot be dropped at later times; they rather need to be kept for the entire duration of computation because they are used in the sums (32)–(33) for reconstructing the overall solution to the AP (38). The latter, in turn, provides a boundary closure for the IP (37).

This strategy, however, may introduce an additional error for the practical implementation of the algorithm. The difficulty is that the accumulating charge is not given by any analytical expression. At every time step, the currents (42)–(43) are

rather constructed from the solution to the IP (37), which is not known ahead of time. Then, the steady-state components of the solution to each partial subproblem can be computed using either (i) the Poisson equation with the charges derived numerically by means of the continuity equations (11) or (ii) the steady-state numerical solution obtained by means of the same scheme taken at a late moment of time when the quasi-lacuna already contains the entire computational domain.

However, neither of these approaches guarantees that the error associated with the computation of an increasing number of steady-state contributions will not accumulate over time. Indeed, each of those steady-state contributions is evaluated numerically, i.e., approximately. Then, we add them together as indicated by the first sum on the right-hand side of (32) and (33), and use for subsequent moments of time as a part of the boundary data for the IP. The number of these approximate steady-state contributions increases over time, which makes it impossible to obtain a temporally uniform error bound. In Sections 6 and 7, we show how to overcome this obstacle and propose a rigorously justified lacunae-based algorithm for combined non-Huygens' problems.

6. Making quasi-lacunae classical

In this section, we show that the partial currents (42)–(43) can be redefined in such a way that the charge accumulated during the operational period of $\boldsymbol{j}_i$ and $\boldsymbol{j}_i^M$ will vanish at every point of the computational domain S:

$$\rho_i = -\int\limits_{iT_1-\Delta T}^{(1+i)T_1} \operatorname{div} \boldsymbol{j}_i \, dt = 0, \quad \rho_i^M = -\int\limits_{iT_1-\Delta T}^{(1+i)T_1} \operatorname{div} \boldsymbol{j}_i^M \, dt = 0.$$

At the same time, the overall solution to the AP obtained by summing up the solutions to individual subproblems will remain unaffected as if it were driven by the original currents (42)–(43). It means that the quasi-lacunae of the partial subproblems will turn into classical lacunae, and one will be able to drop the steady-state components in (32)–(33). This paves the way to a rigorous justification of the algorithm as shown in Section 7.

The following list outlines the main results of this section:

- We propose to redefine the currents (42)–(43) so that their divergence takes the form of a complete time derivative, i.e., $\operatorname{div} \boldsymbol{j}_i = \frac{\partial}{\partial t}(\eta_i \ldots)$, $\operatorname{div} \boldsymbol{j}_i^M = \frac{\partial}{\partial t}(\eta_i \ldots)$. As the compactly supported hat-shaped function $\eta_i = \eta_i(t) = \zeta\,(t-(i-1)T_1)$ is now under the time derivative, the integral of the divergence (i.e., the accumulated charge) over the support of η_i is zero. We achieve that by adding some extra terms to the genuine currents (42)–(43).
- The aforementioned extra terms are proportional to the time derivative $\dot{\eta}_i(t)$ and hence differ from zero only on the overlapping time domain of two neighboring η_i's, see Fig. 5. These additions to the currents generate additional contributions to the field which cancel with one another once assembled into the overall field according to (32)–(33). Hence, adding the terms manually to the currents (42)–(43) yields the same solution of the AP as if the currents were not modified. On the other hand, it is those additional terms that guarantee the desired no-accumulation property.
- The additions to the currents are constructed with the help of the specially chosen auxiliary fields that continuously match the normal components of the actual fields $\boldsymbol{E}$ or $\boldsymbol{H}$ at the boundary of the domain S_0 (see Fig. 6) and are extended inside S_0.
- The aforementioned extension cannot be performed for an arbitrary interior problem. However, our analysis suggests that the proposed method of constructing the currents that remove the accumulation of charge applies to most practical settings.
- We emphasize that the redefined partial currents are not required to be solenoidal on $\mathbb{R}^3$. A theoretical possibility of constructing the solenoidal currents for the AP was pointed out in [23], but its practical implementation faces some unresolved technical issues and computational overheads. On the other hand, the proposed technique of constructing the modified currents that would produce zero charge over their operational period relies on the special structure of the currents (42)–(43). In other words, we do not claim that we can obtain the no-accumulation property for an arbitrary current.

Next, we delineate on the items from the previous list. Altogether, the algorithm for modifying the currents that allows one to avoid the accumulation of charge constitutes a major development on top of our previous approach [23] that uses the original currents (42)–(43). In the end of the section, we also discuss the applicability conditions of the proposed method.

To eliminate the accumulation of charges, we modify the partial currents as follows:

$$\boldsymbol{j}_i(\boldsymbol{x},t) = -\frac{c}{4\pi}\eta_i(t)\left[\frac{1}{c}\frac{\partial \mu \boldsymbol{E}}{\partial t} - \operatorname{curl} \mu \boldsymbol{H}\right] + \frac{1}{4\pi}(1-\mu)\,\dot{\eta}_i(t)\boldsymbol{E}', \tag{49}$$

$$\boldsymbol{j}_i^M(\boldsymbol{x},t) = -\frac{c}{4\pi}\eta_i(t)\left[\frac{1}{c}\frac{\partial \mu \boldsymbol{H}}{\partial t} + \operatorname{curl} \mu \boldsymbol{E}\right] + \frac{1}{4\pi}(1-\mu)\,\dot{\eta}_i(t)\boldsymbol{H}', \tag{50}$$

that is, we add the extra terms:

$$\frac{1}{4\pi}\,(1-\mu)\,\dot{\eta}_i(t)\boldsymbol{E}' \tag{51}$$

and

$$\frac{1}{4\pi}\,(1-\mu)\,\dot{\eta}_i(t)\boldsymbol{H}' \tag{52}$$

to the original expressions (42) and (43), respectively. The upper dot in (51)–(52) denotes differentiation with respect to time, and the auxiliary fields $\boldsymbol{E}'$ and $\boldsymbol{H}'$ are defined as follows:

$$\boldsymbol{E}' = \begin{cases} \boldsymbol{E}, & x \in S_\varepsilon, \\ \boldsymbol{\mathcal{E}}, & x \in S_0, \ \operatorname{div}\boldsymbol{\mathcal{E}} = 0, \end{cases} \qquad \boldsymbol{H}' = \begin{cases} \boldsymbol{H}, & x \in S_\varepsilon, \\ \boldsymbol{\mathcal{H}}, & x \in S_0, \ \operatorname{div}\boldsymbol{\mathcal{H}} = 0. \end{cases} \tag{53}$$

In other words, the fields $\boldsymbol{E}'$ and $\boldsymbol{H}'$ are specified on the computational domain S, and coincide with the fields $\boldsymbol{E}$ and $\boldsymbol{H}$ of the interior problem (37) in the near-boundary layer S_ε. On the bulk of the computational domain, i.e., on S_0, they are obtained by a divergence-free extension: $\operatorname{div}\boldsymbol{\mathcal{E}} = \operatorname{div}\boldsymbol{\mathcal{H}} = 0$ on S_0 for any t. Due to this composite structure, we will refer to the fields (53) as to the composite fields. The divergence of the composite fields is zero both on S_0 and S_ε:

$$\operatorname{div}\boldsymbol{E}' = \operatorname{div}\boldsymbol{H}' = 0, \quad \boldsymbol{x} \in S_0 \ \text{ or } \ \boldsymbol{x} \in S_\varepsilon, \tag{54}$$

because $\operatorname{div}\boldsymbol{E} = \operatorname{div}\boldsymbol{H} = 0$ on S_ε due to (46) and $\operatorname{div}\boldsymbol{\mathcal{E}} = \operatorname{div}\boldsymbol{\mathcal{H}} = 0$ on S_0 by design. We postpone the discussion of a subtle question of how to define and treat the divergence exactly at the boundary ∂S_0 until after we have introduced the matching conditions for the fields on ∂S_0 and proposed the way of actually constructing the extensions $\boldsymbol{\mathcal{E}}$ and $\boldsymbol{\mathcal{H}}$.

In the meantime, assuming that the fields (53) are available, let us analyze the properties of the redefined sources (49)–(50):

1. The extra terms (51)–(52) introduced into the partial currents do not affect the overall solution of the AP. Indeed, the additional terms (51)–(52) differ from zero only on those time intervals where the two consecutive hat-shaped functions $\eta_i(t)$ and $\eta_{i+1}(t)$ overlap and where the time derivative of these functions does not vanish (see Fig. 5). Moreover, on such intervals these consecutive hat functions are related to each other by $\eta_{i+1}(t) = 1 - \eta_i(t)$, so for their time derivatives we have: $\dot{\eta}_{i+1}(t) = -\dot{\eta}_i(t)$. Therefore, the extra terms (51)–(52) in two consecutive partial currents $\boldsymbol{j}_i$, $\boldsymbol{j}_i^M$ and $\boldsymbol{j}_{i+1}$, $\boldsymbol{j}_{i+1}^M$ have equal absolute values but opposite signs. Due to the linearity, these extra terms generate the additional fields (on top of those due to the "unperturbed" currents (42)–(43)) that identically cancel out one another in the sums (32)–(33). In practice, the cancellation occurs with machine precision (as corroborated by numerical simulations of Section 8.4), and it occurs regardless of what the aforementioned additional fields are. In particular, those additional fields may have lower numerical "quality" because the fields $\boldsymbol{E}'$ and $\boldsymbol{H}'$ that provide the corrections (51)–(52) to the right-hand sides (49)–(50) may have their tangential components discontinuous at ∂S_0, see the discussion that follows formula (59). Yet the final quality of the overall finite difference solution stays unaffected because of the identical cancellation of the terms due to the consecutive corrections.
2. The charge accumulated for the operational period of each partial current (49)–(50) is equal to zero. To prove it, consider the divergence of, say, the magnetic current (50):

$$\begin{aligned} \operatorname{div}\boldsymbol{j}_i^M(\boldsymbol{x},t) &= -\frac{\eta_i(t)}{4\pi}\frac{\partial}{\partial t}\operatorname{div}\mu\boldsymbol{H} + \frac{1}{4\pi}\dot{\eta}_i(t)\operatorname{div}(1-\mu)\,\boldsymbol{H}' \\ &= \frac{1}{4\pi}\dot{\eta}_i(t)\operatorname{div}\boldsymbol{H}' - \frac{1}{4\pi}\frac{\partial}{\partial t}\left\{\eta_i(t)\operatorname{div}\mu\boldsymbol{H}'\right\}. \end{aligned} \tag{55}$$

   To derive (55), we used the identity $\operatorname{div}\operatorname{curl} \equiv 0$ and isolated the complete time derivative at the last step. In doing so, we took into account that $\mu\boldsymbol{H} = \mu\boldsymbol{H}'$ everywhere on the computational domain S. It is true on S_ε by design, see (53), and it is true on S_0 because $\mu = 0$ there. Moreover, $\operatorname{div}\boldsymbol{H}' = 0$ due to (54) and thus the divergence (55) takes the form of a complete time derivative. Integrating (55) over the support of the hat function $\eta_i(t)$ at any spatial location within S, we obtain:

$$\rho_i^M = -\int\limits_{iT_1-\Delta T}^{(1+i)T_1} \operatorname{div}\boldsymbol{j}_i^M\,dt = \frac{1}{4\pi}\,\eta_i(t)\operatorname{div}\mu\boldsymbol{H}'\Big|_{iT_1-\Delta T}^{(1+i)T} = 0, \tag{56}$$

   because $\eta_i(t)$ vanishes at the endpoints $t = (1+i)T$ and $t = iT_1 - \Delta t$. The same applies to the electric current (49).
3. The modified currents (49)–(50) are no longer localized inside the near-boundary layer S_ε (as opposed to the original currents (42)–(43)), see Fig. 6, because the additional terms (51)–(52) do not, generally speaking, vanish on S_0. Indeed, the extensions $\boldsymbol{\mathcal{E}}$ and $\boldsymbol{\mathcal{H}}$ are basically non-zero on S_0 and besides, $1-\mu = 1$ there. Still, in order to construct the

currents (49)–(50) at a given moment of time, one needs to know the solution of the interior problem, i.e., the values of the fields $\boldsymbol{E}$ and $\boldsymbol{H}$, only on S_ε. Then, these fields are extended inside S_0 in a certain way, which yields the fields $\boldsymbol{\mathcal{E}}$, $\boldsymbol{\mathcal{H}}$ in (53).

4. While the currents (49)–(50) are, generally speaking, non-zero on the computational domain S, they turn into zero outside S (including the boundary $\Gamma = \partial S$) because the original currents (42)–(43) do so and the extra terms (51)–(52) vanish on $\mathbb{R}^3 \backslash S$ as $1 - \mu = 0$ there.

Let us now explain how to construct the extensions $\boldsymbol{\mathcal{E}}$ and $\boldsymbol{\mathcal{H}}$ in practice. Given the values of $\boldsymbol{E}$ and $\boldsymbol{H}$ on the boundary ∂S_0 for any t, we seek the extensions $\boldsymbol{\mathcal{E}}$, $\boldsymbol{\mathcal{H}}$ in the form of anti-gradients of the respective potentials that solve the Neumann problem for the Laplace equation on S_0:

$$\begin{cases} \Delta\varphi = 0, \\ \left.\dfrac{\partial\varphi}{\partial n}\right|_{\partial S_0} = -E_n, \end{cases} \qquad \begin{cases} \Delta\varphi^M = 0, \\ \left.\dfrac{\partial\varphi^M}{\partial n}\right|_{\partial S_0} = -H_n, \end{cases} \qquad \boldsymbol{x} \in S_0, \tag{57}$$

$$\boldsymbol{\mathcal{E}} = -\nabla\varphi, \quad \boldsymbol{\mathcal{H}} = -\nabla\varphi^M. \tag{58}$$

In formulae (57)–(58), φ, φ_M are the unknown potentials, $\frac{\partial}{\partial n}$ is the normal derivative on ∂S_0, and E_n, H_n are the normal components of the fields $\boldsymbol{E}$, $\boldsymbol{H}$ of the interior problem (37) on ∂S_0.

Clearly, the fields $\boldsymbol{\mathcal{E}}$ and $\boldsymbol{\mathcal{H}}$ constructed according to (57)–(58) are solenoidal because

$$\begin{aligned} &\operatorname{div}\boldsymbol{\mathcal{E}} = -\operatorname{div}\nabla\varphi \equiv -\Delta\varphi = 0, \\ &\operatorname{div}\boldsymbol{\mathcal{H}} = -\operatorname{div}\nabla\varphi^M \equiv -\Delta\varphi^M = 0. \end{aligned} \tag{59}$$

Relations (59) hold everywhere on S_0 up to the boundary.

The boundary conditions in (57) are set for the normal derivative of the potential rather than for the potential itself because it is the fields $\boldsymbol{E}$ and $\boldsymbol{H}$ that are assumed known on ∂S_0. These conditions guarantee the continuity of the normal components of the composite fields (53) on the interface ∂S_0 but say nothing about their tangential components. Then, the tangential components will, generally speaking, remain discontinuous on ∂S_0. In that regard we note that the problem of constructing a solenoidal extension for a given vector field can also be solved in a stricter formulation that requires the continuity of both the normal and tangential components, see [28, Chapter 1, Section 2]. There are, in fact, multiple solutions to such a problem for a domain bounded by a Lyapunov surface (the surface that has a Hölder-continuous normal). Our construct (57)–(58) that guarantees the continuity of the normal component is actually a part of the overall field that can be built according to [28]. The other part that would guarantee the continuity of the tangential component is obtained in [28] in the form of the curl of an auxiliary field. The extension of the results of [28] to a surface with lower regularity, as well as their transition to the discrete framework with subsequent estimate of complexity, may be less than straightforward. At the same time, our simple and inexpensive approach (57)–(58) yields exactly as much as needed for a successful implementation of the algorithm — a continuous normal component of the extension that, in turn, guarantees the continuity of the divergence. In doing so, the continuity of the tangential components is needed neither in theory nor in practice, see item 1 on page 15.

The discontinuity of the tangential components though does not lead to discontinuity of the divergence of the composite fields $\boldsymbol{E}'$ and $\boldsymbol{H}'$ on the boundary ∂S_0, or, more precisely, does not make the divergence singular. Indeed, when calculating the divergence, normal components of the fields are differentiated along the normal direction whereas the tangential components are differentiated along the tangential directions. Therefore, even as the tangential components undergo jumps at ∂S_0, all differentiations can be carried through independently on different sides of the interface ∂S_0, and the resulting quantities will be bounded. Hence, the divergence of $\boldsymbol{E}'$ or $\boldsymbol{H}'$ can formally be considered a dual-valued function on ∂S_0. As, however, both values coincide, see (54), we can define this divergence on ∂S_0 merely by continuity, and consider $\operatorname{div}\boldsymbol{E}' = \operatorname{div}\boldsymbol{H}' = 0$ for all $\boldsymbol{x} \in S$.

Let us re-emphasize that the extension of the true fields $\boldsymbol{E}$ and $\boldsymbol{H}$ from S_ε to S_0 by means of $\boldsymbol{\mathcal{E}}$ and $\boldsymbol{\mathcal{H}}$, respectively, see formulae (53), can be quite arbitrary as along as it satisfies the main requirement — that the divergence of both $\boldsymbol{E}'$ and $\boldsymbol{H}'$ be continuous and, in fact, equal to zero on the entire domain S. This requirement, in turn, guarantees that the modified currents (49)–(50) will not accumulate the charge. The specific approach that we have chosen for building $\boldsymbol{\mathcal{E}}$ and $\boldsymbol{\mathcal{H}}$ is based on solving the Neumann problems (57) and subsequently computing the gradients (58). As we have explained earlier, this choice is not unique. We use it because it serves the purpose despite the possible tangential discontinuity at ∂S_0 and proves inexpensive and easy to implement otherwise. In doing so, the resulting extended fields $\boldsymbol{E}'$ and $\boldsymbol{H}'$ coincide with the true fields $\boldsymbol{E}$ and $\boldsymbol{H}$ only on S_ε, whereas on S_0 the fields $\boldsymbol{E}'$ and $\boldsymbol{H}'$ shall be interpreted as auxiliary quantities that, in particular, may have nothing to do with the true fields of the IP on S_0.

The additional cost associated with computing the corrections (51)–(52) is not expected to be large. First of all, problems (57) need to be solved only on those intervals of time where the function $\eta_i(t)$ varies, because the corrections (51)–(52) are proportional to $\dot{\eta}_i(t)$. In practice, those intervals constitute a small fraction (5%–10%) of the overall duration T_0 of a given partition element, see Fig. 5. Moreover, problems (57) are solved very efficiently by means of the FFT, which helps keep the

overall complexity almost the same as that of an explicit time-marching scheme (i.e., almost linear). Finally, very often it is sufficient to perform the reduction of quasi-lacunae to classical lacunae only for one field, electric or magnetic, rather than for both fields, and accordingly, solve only one of the two systems (57). This is an implication of the fact that the boundary conditions for the interior problem are typically set either for the electric field or for the magnetic field. We discuss these questions on page 18 and also in Section 8.3 on page 25.

Each of the interior Neumann problems for the Laplace equation, see (57), is known to have a solution only if the corresponding compatibility condition holds for the boundary data [29]:

$$\Phi = \int\limits_{\partial S_0} E_n dS = 0, \quad \Phi^M = \int\limits_{\partial S_0} H_n dS = 0. \tag{60}$$

In other words, problems (57) are solvable only if the fluxes of the fields $\boldsymbol{E}$ and $\boldsymbol{H}$ through the surface ∂S_0 are equal to zero. The solutions to (57) are unique but, obviously, up to an additive constant. The extensions $\boldsymbol{\mathcal{E}}$ and $\boldsymbol{\mathcal{H}}$ are unique in the strict sense because the differentiation of φ, φ^M in (58) eliminates that arbitrary constant. Due to the constraint (60), the solenoidal (divergence-free) extension that we have described may not exist for any given interior problem (37). Hereafter, we discuss some specific cases where the extension can still be obtained.

To begin with, we emphasize that conditions (60) are necessary for the solenoidal extensions of the given vector fields $\boldsymbol{E}$ and $\boldsymbol{H}$ onto the domain S_0 to exist in the form (57)–(58). In the context of our discussion, $\boldsymbol{E}$ and $\boldsymbol{H}$ are the electric and magnetic field of a potentially sophisticated interior problem (37). Those fields may display some complex behavior, and may, in particular, not even be defined everywhere on S_0 if, e.g., there are impenetrable scattering objects inside the computational domain. Therefore, equalities (60), which can be checked if the fields are known only outside S_0, is all that tells us about the possibility of building the desired extensions $\boldsymbol{\mathcal{E}}$ and $\boldsymbol{\mathcal{H}}$. If, however, the interior problem is made a little more specific, then it appears possible to identify some narrower yet perfectly meaningful classes of formulations to which conditions (60) will apply.

First of all, the extension will be needed for all those intervals of time where the functions $\eta_i(t)$ that render the partition of unity (see Fig. 5) vary. Hence, we supply the argument t to all the quantities involved, e.g., $\boldsymbol{E} = \boldsymbol{E}(t)$ and $\boldsymbol{H} = \boldsymbol{H}(t)$. Next, keeping in mind that $\boldsymbol{E}(t)$ and $\boldsymbol{H}(t)$ are the electric and magnetic fields, we recast conditions (60) in terms of the total charge of the system:

$$0 = \Phi(t) = \int\limits_{\partial S_0} E_n(t) dS = \int\limits_{S_0} \operatorname{div} \boldsymbol{E}(t) d\boldsymbol{x} = 4\pi \int\limits_{S_0} \rho(t) d\boldsymbol{x} \equiv 4\pi\, Q(t), \tag{61}$$

$$0 = \Phi^M(t) = \int\limits_{\partial S_0} H_n(t) dS = \int\limits_{S_0} \operatorname{div} \boldsymbol{H}(t) d\boldsymbol{x} = 4\pi \int\limits_{S_0} \rho^M(t) d\boldsymbol{x} \equiv 4\pi\, Q^M(t), \tag{62}$$

where we have applied the Gauss theorem to the domain S_0 and also employed the Gauss laws (13). Hence, the possibility to obtain a solenoidal extension at any given moment of time depends on whether or not the total electric charge $Q(t)$ or magnetic charge $Q^M(t)$ is zero.

Furthermore, recall that we are considering only "isolated" systems of type (37) surrounded by vacuum, see (35). Hence, there can be no transport of charge (i.e., no current) from the exterior of S_0. Therefore, the total charge is conserved, i.e., $Q(t) = Q(0) = \text{const}$, $Q^M(t) = Q^M(0) = \text{const}$.

Let us now make the IP more specific by identifying it with a lossy Maxwell's system driven by the extraneous current $\boldsymbol{j}$ and having the conductivity σ:

$$\operatorname{curl} \boldsymbol{H} = \frac{1}{c} \frac{\partial \boldsymbol{E}}{\partial t} + \frac{4\pi}{c} (\boldsymbol{j} + \sigma \boldsymbol{E}), \tag{63}$$

$$\operatorname{curl} \boldsymbol{E} = -\frac{1}{c} \frac{\partial \boldsymbol{H}}{\partial t}. \tag{64}$$

Both $\boldsymbol{j}$ and σ in the Ampère law (63) are almost arbitrary except that they are required to turn into zero outside S_0. Taking the divergence of (63) and (64) and integrating over S_0 we obtain

$$\frac{\partial}{\partial t} \int\limits_{\partial S_0} E_n dS = -\frac{4\pi}{c} \int\limits_{\partial S_0} (j_n + \sigma E_n)\, dS, \tag{65}$$

$$\frac{\partial}{\partial t} \int\limits_{\partial S_0} H_n dS = 0, \tag{66}$$

where we have also used the Gauss theorem. Since under our assumption the current $\boldsymbol{j}$ and conductivity σ vanish on ∂S_0, we have from (65):

$$\int\limits_{\partial S_0} E_n(t)dS = \text{const} \equiv 4\pi\, Q\,(0). \tag{67}$$

Similarly, taking into account that there is no magnetic charge in a real life physical setting, $\rho^M = 0$, we obtain from (66):

$$\int\limits_{\partial S_0} H_n(t)dS = 0. \tag{68}$$

Comparing (67) to the first condition (60), we conclude that for a realistic IP of the type (63)–(64) the possibility of building a solenoidal extension of the electric field $\boldsymbol{E}$ onto S_0 in the form (57)–(58) is time invariant and is determined only by whether the conserved total electric charge is zero.

Let us point out some special yet practically relevant situations when a divergence-free extension of the electric field can be constructed:

- A wide class of problems with zero initial conditions for $\boldsymbol{E}$. Clearly, if the total charge were not zero the IP would generate an electrostatic field contrary to the assumption $\boldsymbol{E}(0) = \boldsymbol{0}$. Mathematically, integrating $\operatorname{div} \boldsymbol{E}(0) = 4\pi\rho(0) = 0$ over S_0 we obtain zero total charge.
- On the other hand, the condition $\boldsymbol{E}(0) = \boldsymbol{0}$ is sufficient but not necessary for building a divergence-free extension. Indeed, we can consider a system with zero total charge but non-vanishing higher multipole moments (dipole, quadrupole, etc.). Such system still generates the electrostatic field yet as there is no total charge and the divergence-free extension is possible.

It is also important to emphasize that the magnetic field can always be extended onto S_0 in a divergence-free way due to (68). Indeed, as there are no physical magnetic charges, the second condition (60) written in the form (62) will always hold. The previous version of our algorithm [23] did not allow us to take advantage of that because it employed the non-physical auxiliary magnetic charges and the quasi-lacunae, as opposed to genuine lacunae, for the magnetic field. In the current version of the algorithm, if the AP and the IP are coupled via the magnetic field, then one can always guarantee that the error won't accumulate due to the use of the classical lacunae. In that regard we note that while the choice of the field to be used for coupling depends on what scheme is employed to discretize the Maxwell equations and how it is implemented, there is still a substantial degree of flexibility. This flexibility can often be exercised to build a formulation that requires the outer boundary conditions only for the magnetic field. In this case, there will be no limitations whatsoever for the class of problems that the proposed methodology will apply to.

If the AP and IP are coupled or need to be coupled via the electric field (for example, this is the approach adopted in Section 8.3), then the proposed methodology does have a limitation that can be expressed in terms of zero flux or zero total charge, see formulae (60) and (61). Our previous discussion shows that the class of formulations that can be addressed in this framework is still sufficiently broad. At the same time, the benefit of using the methodology is its provably non-deteriorating behavior over long times (see Section 7). Moreover, the nature of the limitation is algorithmic rather than fundamental, and in the future we will look into how to alleviate it.

We conclude this section by summarizing the results on the solenoidal extension (57)–(58):

- For the general IP, one can obtain a divergence-free extension of $\boldsymbol{E}$ or $\boldsymbol{H}$ into S_0 only if the flux of the respective field through S_0 is zero at any t.
- For all physical IPs, a divergence-free extension of the magnetic field is possible. This result alone already allows us to eliminate the steady-state components of the field inside the lacunae and hence construct a lacunae-based algorithm with a theoretically justified temporally uniform error bound.
- For isolated physical IPs, a divergence-free extension of the electric field can be built in the form (57)–(58) provided that the conserved total electric charge is zero.

7. A temporally uniform error bound

In this section, we prove a temporally uniform estimate for the error which is due to the treatment of the artificial outer boundary in the case where the lacunae-based time marching is applied to a non-Huygens' problem. If the computational domain is terminated by an ABC or a PML, then the lacunae based time marching facilitates its non-deteriorating behavior over arbitrarily long times. Qualitatively, the mechanism of the non-deteriorating performance is very simple. The partial subproblems that compose the AP need to be integrated only over a limited interval of time during which the intrinsic instabilities of the ABC/PML, if any, do not develop.

The proof of the temporally uniform error bound relies on the modified auxiliary currents of Section 6 or, equivalently, on the use of classical lacunae as opposed to quasi-lacunae. In that regard we note that the time-marching strategy based

on quasi-lacunae, see [23], allows one to prove a temporally uniform error estimate only when the currents and charges that drive the field are known ahead of time, which is not the case for a non-Huygens' setting, see Section 5.

We first recall that under our approach an ABC or PML is applied to the auxiliary problem (38). Hence, it is sufficient to demonstrate that the error introduced by the ABC/PML into the solution of the AP will stay bounded for all times. This, in turn, implies that the same error bound will apply to the IP (37) because the latter takes the solution of the AP as the boundary data.

The governing equations of the AP (38) read:

$$\begin{aligned} &\frac{1}{c}\frac{\partial \boldsymbol{w}^{\text{aux}}}{\partial t} + \hat{\mathbf{L}}\boldsymbol{w}^{\text{aux}} = \boldsymbol{f}^{\text{aux}}(\boldsymbol{x},t), \quad \boldsymbol{x}\in\mathbb{R}^3, \quad t>0, \\ &\boldsymbol{w}^{\text{aux}}(\boldsymbol{x},0) = \mathbf{0}, \quad \boldsymbol{x}\in\mathbb{R}^3, \end{aligned} \tag{69}$$

where

$$\boldsymbol{f}^{\text{aux}}(\boldsymbol{x},t) = -\tfrac{4\pi}{c}\left[\boldsymbol{j}, \boldsymbol{j}^{\text{M}}\right]^T$$

and

$$\hat{\mathbf{L}} = \begin{bmatrix} 0 & -\text{curl} \\ \text{curl} & 0 \end{bmatrix}.$$

Even though problem (69) is posed on the entire $\mathbb{R}^3$, for practical implementation one has to reformulate it on a bounded domain. It will be convenient to use the same domain S as the one we introduced for decomposition, see Fig. 6:

$$\begin{aligned} &\frac{1}{c}\frac{\partial \boldsymbol{w}^{(S)}}{\partial t} + \hat{\mathbf{L}}\boldsymbol{w}^{(S)} = \boldsymbol{f}^{\text{aux}}(\boldsymbol{x},t), \quad \boldsymbol{x}\in S, \ t>0, \\ &\hat{\boldsymbol{\Gamma}}\boldsymbol{w}^{(S)}(\boldsymbol{x},t) = \mathbf{0}, \quad \boldsymbol{x}\in\Gamma, \ t>0, \\ &\boldsymbol{w}^{(S)}(\boldsymbol{x},0) = \mathbf{0}, \quad \boldsymbol{x}\in S. \end{aligned} \tag{70}$$

The operator $\hat{\boldsymbol{\Gamma}}$ in formula (70) represents the ABC or PML set at the outer boundary $\Gamma = \partial S$.

For an ideal ABC or PML, the solutions to problems (69) and (70) coincide on S:

$$\boldsymbol{w}^{\text{aux}}(\boldsymbol{x},t) \equiv \boldsymbol{w}^{(S)}(\boldsymbol{x},t), \quad \boldsymbol{x}\in S, \tag{71}$$

for any moment of time $t>0$. In practice, however, no ABC or PML is ideal, and instead of equality (71) the following inequality holds:

$$\|\boldsymbol{w}(\boldsymbol{x},t) - \boldsymbol{w}^{(S)}(\boldsymbol{x},t)\| \leqslant \delta(\hat{\boldsymbol{\Gamma}}), \quad \boldsymbol{x}\in S. \tag{72}$$

The constant δ on the RHS of (72) depends on the operator $\hat{\boldsymbol{\Gamma}}$, i.e., on the quality of the ABC or PML at ∂S. The norm $\|\cdot\|$ in formula (72) and thereafter can be any appropriate function norm in space, so that the left-hand side of inequality (72) depends only on the time t. In the ideal case, $\delta = 0$, and then (72) transforms into (71). Otherwise, δ is non-zero; in the case of an ABC it may depend, for example, on the order of the boundary condition (see, e.g., [11,13,17]), whereas in the case of a PML it may depend, in particular, on its thickness and the absorption profile. In all the cases, however, a non-deteriorating long-time performance implies that δ does not depend on time, or more precisely, remains bounded as the time elapses.

Yet this is not always the case. To account for the possible adverse behavior, we interpret any long-time error growth as the growth of small perturbations in the data that drive the problem, see [4]. Specifically, along with the actual solution $\boldsymbol{w}^{(S)}$ that satisfies system (70) on the bounded region S, we consider its perturbed counterpart $\tilde{\boldsymbol{w}}^{(S)}$ that satisfies the system with the perturbed boundary data, initial data, and the RHS:

$$\begin{aligned} &\frac{1}{c}\frac{\partial \tilde{\boldsymbol{w}}^{(S)}}{\partial t} + \hat{\mathbf{L}}\tilde{\boldsymbol{w}}^{(S)} = \boldsymbol{f}^{\text{aux}}(\boldsymbol{x},t) + \boldsymbol{\mu}, \quad \boldsymbol{x}\in S, \ t>0, \\ &\hat{\boldsymbol{\Gamma}}\tilde{\boldsymbol{w}}^{(S)}(\boldsymbol{x},t) = \boldsymbol{\epsilon}, \quad \boldsymbol{x}\in\partial S, \ t>0, \\ &\tilde{\boldsymbol{w}}^{(S)}(\boldsymbol{x},0) = \boldsymbol{\xi}, \quad \boldsymbol{x}\in S. \end{aligned} \tag{73}$$

The difference between the perturbed and unperturbed solutions on the domain S may grow as the time t elapses:

$$\|\tilde{\boldsymbol{w}}^{(S)}(\boldsymbol{x},t) - \boldsymbol{w}^{(S)}(\boldsymbol{x},t)\| \leqslant \eta(t)\,\|[\boldsymbol{\mu},\boldsymbol{\epsilon},\boldsymbol{\xi}]\|'. \tag{74}$$

The rate of growth $\eta(t)$ is determined by the particular ABC or PML; for example, some well-known PMLs have been reported to demonstrate a linear or quadratic growth [2,5,4]. The notation $[\boldsymbol{\mu},\boldsymbol{\epsilon},\boldsymbol{\xi}]$ on the RHS of inequality (74) represents

a symbolic vector of all perturbations of the data in system (73). The choice of norms $\|\cdot\|$ and $\|\cdot\|'$ for some specific cases is discussed in [2,5,4]. Inequality (74) is general in the sense that it allows the perturbations of the data to grow with a prescribed rate, yet the reason for the growth may be arbitrary and it does not need to be known.

Inequality (74) implies that the perturbations that are small initially may increase with no bound for large integration times. If, however, the plain integration of system (70) is replaced by the lacunae-based time marching similar to that described in Section 4 but based on the modified partial currents (49)–(50), then estimate (74) can be made uniform in time. Indeed, both solutions, $\boldsymbol{w}^{(S)}(\boldsymbol{x},t)$ and $\tilde{\boldsymbol{w}}^{(S)}(\boldsymbol{x},t)$, can be partitioned similarly to how it is done in formulae (32)–(33), but with no steady-state contributions, because unlike the original currents (42)–(43), the modified currents (49)–(50) do not lead to the accumulation of charge, see formula (56). Accordingly, the quasi-lacunae transform into classical lacunae, for which the solution behind the aft fronts is zero. Hence, we have:

$$\boldsymbol{w}^{(S)}(\boldsymbol{x},t)=\sum_{i=N_0}^{N_1}\boldsymbol{w}_i^{(S)}(\boldsymbol{x},t), \tag{75}$$

$$\tilde{\boldsymbol{w}}^{(S)}(\boldsymbol{x},t)=\sum_{i=N_0}^{N_1}\tilde{\boldsymbol{w}}_i^{(S)}(\boldsymbol{x},t). \tag{76}$$

Since each term on the right-hand side of either (75) or (76) needs to be integrated only for a limited time T_{int}, see formula (27), estimate (74) yields for $i=N_0,\ldots,N_1$:

$$\|\tilde{\boldsymbol{w}}_i^{(S)}(\boldsymbol{x},t)-\boldsymbol{w}_i^{(S)}(\boldsymbol{x},t)\|\leqslant C_0\|[\boldsymbol{\mu}_i,\boldsymbol{\epsilon}_i,\boldsymbol{\xi}_i]\|', \tag{77}$$

where $C_0=\eta(T_{\text{int}})$ is a constant, and $[\boldsymbol{\mu}_i,\boldsymbol{\epsilon}_i,\boldsymbol{\xi}_i]$ denotes perturbations of the data for the i-th partial problem. As the overall number of unsteady terms N_1-N_0+1 in either sum (75) or (76) does not exceed the value $\left[\frac{\operatorname{diam} S/c}{T_0}\right]+2$ for all times, we can use the triangle inequality and obtain the following estimate for the functions (75) and (76):

$$\left\|\boldsymbol{w}^{(S)}(\boldsymbol{x},t)-\tilde{\boldsymbol{w}}^{(S)}(\boldsymbol{x},t)\right\|=\left\|\sum_{i=N_0}^{N_1}\tilde{\boldsymbol{w}}_i^{(S)}(\boldsymbol{x},t)-\sum_{i=N_0}^{N_1}\boldsymbol{w}_i^{(S)}(\boldsymbol{x},t)\right\|\leqslant C_1\sup_i\left\|[\boldsymbol{\mu}_i,\boldsymbol{\epsilon}_i,\boldsymbol{\xi}_i]\right\|'. \tag{78}$$

In formula (78), $C_1=C_0\cdot\left(\left[\frac{\operatorname{diam} S/c}{T_0}\right]+2\right)$, and the supremum on the right-hand side of inequality (78) can be assumed bounded. Finally, combining estimates (72) and (78) with the help of the triangle inequality, we arrive at the following result.

Theorem 2. *Let $S\subset\mathbb{R}^3$ be a bounded computational domain, and let problem (69) be solved on S using an appropriate ABC or PML that reduces it to problem (70). Let problem (70) be time marched with the help of classical lacunae, i.e., using the modified auxiliary sources (49)–(50). Then, assuming that $\sup_i\|[\boldsymbol{\mu}_i,\boldsymbol{\epsilon}_i,\boldsymbol{\xi}_i]\|'<\infty$, the error on the computational domain S will remain uniformly bounded for all times:*

$$\|\tilde{\boldsymbol{w}}^{(S)}(\boldsymbol{x},t)-\boldsymbol{w}(\boldsymbol{x},t)\|\leqslant\delta(\hat{\boldsymbol{\Gamma}})+C_1\sup_i\|[\boldsymbol{\mu}_i,\boldsymbol{\epsilon}_i,\boldsymbol{\xi}_i]\|'. \tag{79}$$

Theorem 2 guarantees that regardless of what causes the original long-time deterioration, time-marching with the help of classical lacunae will prevent any possible error growth.

We conclude this section by noting that had the algorithm been based on the original currents (42)–(43) rather than the modified currents (49)–(50), and hence on quasi-lacunae as opposed to classical lacunae, then the sums (75) and (76) would have contained the non-zero steady-state contributions, similarly to the sums (32) and (33):

$$\boldsymbol{w}^{(S)}(\boldsymbol{x},t)=\sum_{i=0}^{N_0-1}\boldsymbol{w}_i^{(S),\text{st}}(\boldsymbol{x})+\sum_{i=N_0}^{N_1}\boldsymbol{w}_i^{(S)}(\boldsymbol{x},t), \tag{75$'$}$$

$$\tilde{\boldsymbol{w}}^{(S)}(\boldsymbol{x},t)=\sum_{i=0}^{N_0-1}\tilde{\boldsymbol{w}}_i^{(S),\text{st}}(\boldsymbol{x})+\sum_{i=N_0}^{N_1}\tilde{\boldsymbol{w}}_i^{(S)}(\boldsymbol{x},t). \tag{76$'$}$$

Since the currents (42)–(43) are not given ahead of time and rather evaluated concurrently with the solution, all steady-state contributions on the right-hand side of (75′) and (76′) need to be computed numerically at the appropriate moments of time. A most straightforward way to do so is to take them as the residual fields inside the quasi-lacunae for each $i=0,\ldots,N_0-1$. Accordingly, the sums of the steady-state contributions in (75′)–(76′) cannot be replaced with one cumulative contribution at the final moment of time (see the discussion to that effect in the end of Section 4).

Using formulae (75′) and (76′), we can write:

$$\left\| \boldsymbol{w}^{(S)}(\boldsymbol{x},t) - \tilde{\boldsymbol{w}}^{(S)}(\boldsymbol{x},t) \right\| \leqslant \left\| \sum_{i=0}^{N_0-1} \tilde{\boldsymbol{w}}_i^{(S),\mathrm{st}} - \sum_{i=0}^{N_0-1} \boldsymbol{w}_i^{(S),\mathrm{st}} \right\| + \left\| \sum_{i=N_0}^{N_1} \tilde{\boldsymbol{w}}_i^{(S)}(\boldsymbol{x},t) - \sum_{i=N_0}^{N_1} \boldsymbol{w}_i^{(S)}(\boldsymbol{x},t) \right\|. \tag{80}$$

The second norm on the right-hand side of inequality (80) can still be estimated according to (78). However, the expression under the first norm contains the steady-state terms computed numerically, and their number N_0 increases as the time elapses. As each of those terms carries a certain error, one cannot use (80) to prove an overall temporally uniform error bound similar to (78) or (79).

An alternative strategy to obtain the steady-state component of the solution in (75′) or (76′) could be to integrate the continuity equations (11) in time with the currents given by (42)–(43), and then solve the Poisson equations (25)–(26). However, the time marching of ODEs is also prone the accumulation of error, and this will subsequently contaminate the potentials obtained by solving equations (25)–(26). One scenario for which this does not happen is when the currents and charges that drive the Maxwell equations are known analytically. This, however, is not the case for the combined IP/AP formulation described in Section 5. On the other hand, the approach of Section 6 that transforms the quasi-lacunae back to classical lacunae guarantees that the error associated with the domain truncation will stay bounded for all times, see Theorem 2.

8. Implementation and numerical experiments

In this section, we present the numerical results that corroborate the performance of the proposed lacunae-based methodology. The interior problem that we have chosen consists of solving the inhomogeneous Maxwell's equations in the spherical transverse magnetic (TM) mode. The corresponding solution is axially symmetric with respect to the z axis so that none of the functions involved depends on the azimuthal angle φ. The non-zero components of the electromagnetic field in the spherical coordinates (r,θ,φ) are E_r, E_θ, and H_φ. This configuration is simple yet it presents no loss of generality, because our numerical solver does not rely on any special properties of the solution and rather computes it in the full three-dimensional setting.

Specifically, we are solving the 3D Maxwell equations in the Cartesian coordinates:

$$\frac{\partial H_z}{\partial y} - \frac{\partial H_y}{\partial z} = \frac{1}{c}\frac{\partial E_x}{\partial t} + \frac{4\pi}{c} j_x, \tag{81}$$

$$-\frac{\partial H_z}{\partial x} + \frac{\partial H_x}{\partial z} = \frac{1}{c}\frac{\partial E_y}{\partial t} + \frac{4\pi}{c} j_y, \tag{82}$$

$$\frac{\partial H_y}{\partial x} - \frac{\partial H_x}{\partial y} = \frac{1}{c}\frac{\partial E_z}{\partial t} + \frac{4\pi}{c} j_z, \tag{83}$$

$$\frac{\partial E_z}{\partial y} - \frac{\partial E_y}{\partial z} = -\frac{1}{c}\frac{\partial H_x}{\partial t}, \tag{84}$$

$$\frac{\partial E_x}{\partial z} - \frac{\partial E_z}{\partial x} = -\frac{1}{c}\frac{\partial H_y}{\partial t}, \tag{85}$$

$$\frac{\partial E_y}{\partial x} - \frac{\partial E_x}{\partial y} = -\frac{1}{c}\frac{\partial H_z}{\partial t}, \tag{86}$$

subject to zero initial conditions. While our test solution is axially symmetric and also has $H_z \equiv 0$, system (81)–(86) is integrated in its original intact form. This allows us to demonstrate in practice the regularization capabilities of the lacunae-based methodology over long times in 3D. To do so, we choose the computational domain S shaped as a cube with side $2a$:

$$S = \{(x,y,z):\ -a \leqslant x,y,z \leqslant a\}, \tag{87}$$

and set the unsplit PML of [30] at its outer boundary ∂S. This PML sustains stable behavior and provides good accuracy over moderate simulation times yet may lead to a blow-up of the solution at longer runs. The long time deterioration may be attributed to the near-edge and near-corner regions of the computational domain in three dimensions.

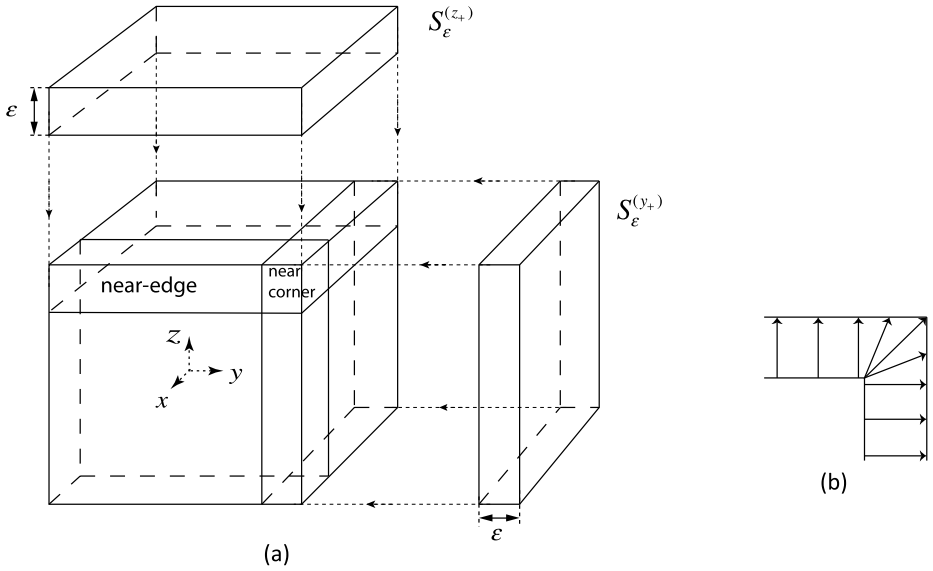

Fig. 7. (a) The near-boundary layer S_ε (only two of the six planar layers (88)–(93) are shown); (b) The direction of growth of μ in the near-edge region.

8.1. Auxiliary problem

The overall auxiliary problem is partitioned into subproblems that require solving the same Maxwell system (81)–(86) but driven by the electric currents $\boldsymbol{j}_i$ of (49) and magnetic currents $\boldsymbol{j}_i^M$ of (43). We do not use the modified magnetic currents (50) because we implement a particular version of the algorithm (see Section 8.3) where the boundary conditions are set only for the electric field and hence the classical lacunae (in the sense of Section 6) are needed only for the electric field as well. The function μ is a part of the definition of the currents (49) and (43). It varies smoothly between 0 to 1 on the region S_ε, which is a thin layer on the interior side of ∂S, see Fig. 6. Given that the computational domain S is shaped as a cube, see (87), we define the set S_ε as the union of six planar layers of width ε adjacent to the outer boundaries $x=\pm a$, $y=\pm a$, and $z=\pm a$ of S:

$$S_\varepsilon = S_\varepsilon^{(x_+)} \cup S_\varepsilon^{(x_-)} \cup S_\varepsilon^{(y_+)} \cup S_\varepsilon^{(y_-)} \cup S_\varepsilon^{(z_+)} \cup S_\varepsilon^{(z_-)},$$

where

$$S_\varepsilon^{(x_+)} = \{a-\varepsilon \leqslant x \leqslant a,\ -a \leqslant y \leqslant a,\ -a \leqslant z \leqslant a\}, \tag{88}$$

$$S_\varepsilon^{(x_-)} = \{-a \leqslant x \leqslant -a+\varepsilon,\ -a \leqslant y \leqslant a,\ -a \leqslant z \leqslant a\}, \tag{89}$$

$$S_\varepsilon^{(y_+)} = \{-a \leqslant x \leqslant a,\ a-\varepsilon \leqslant y \leqslant a,\ -a \leqslant z \leqslant a\}, \tag{90}$$

$$S_\varepsilon^{(y_-)} = \{-a \leqslant x \leqslant a,\ -a \leqslant y \leqslant -a+\varepsilon,\ -a \leqslant z \leqslant a\}, \tag{91}$$

$$S_\varepsilon^{(z_+)} = \{-a \leqslant x \leqslant a,\ -a \leqslant y \leqslant a,\ a-\varepsilon \leqslant z \leqslant a\}. \tag{92}$$

$$S_\varepsilon^{(z_-)} = \{-a \leqslant x \leqslant a,\ -a \leqslant y \leqslant a,\ -a \leqslant z \leqslant -a+\varepsilon\}. \tag{93}$$

The layers (88)–(93) partially overlap near the edges and corners of S_ε, see Fig. 7(a).

The function $\mu = \mu(\boldsymbol{x})$ that helps us define the auxiliary currents, see formulae (39)–(41), is introduced with the help of the following single-variable function, which is a composition of a seventh degree polynomial and two constants:

$$P_4(x) = \begin{cases} 0, & x \leqslant 0, \\ 35x^4 - 84x^5 + 70x^6 - 20x^7, & 0 \leqslant x \leqslant 1, \\ 1, & x \geqslant 1. \end{cases} \tag{94}$$

The function (94) is continuous itself and has continuous derivatives up to order for $-\infty < x < \infty$. It can be thought of as a "smoothed" step function extended to the interval $[0,1]$.

On the non-overlapping parts of S_ε, the function μ smoothly grows from 0 to 1 in the direction of the outer normal to a given layer. For example, for the non-overlapping part of $S_\varepsilon^{(x_+)}$ we define:

$$\mu(x,y,z) \stackrel{\text{def}}{=} P_4\left(\frac{x-a+\varepsilon}{\varepsilon}\right), \quad (x,y,z) \in S_\varepsilon^{(x_+)} \backslash \{S_\varepsilon^{(y_+)} \cup S_\varepsilon^{(z_+)} \cup S_\varepsilon^{(y_-)} \cup S_\varepsilon^{(z_-)}\},$$

and similarly for the non-overlapping parts of $S_\varepsilon^{(x_-)}$, $S_\varepsilon^{(y_\pm)}$, $S_\varepsilon^{(z_\pm)}$.

On the near-edge regions where two layers overlap, the direction of growth makes a smooth 90° turn (see Fig. 7(b)), and μ grows there as a function of the distance from the edge, for example:

$$\mu(x,y,z) = P_4\left(\frac{r_{xz}}{\varepsilon}\right), \quad r_{xz} = \sqrt{(x-a+\varepsilon)^2 + (z-a+\varepsilon)^2},$$
$$(x,y,z) \in S_\varepsilon^{(x_+)} \cap S_\varepsilon^{(z_+)} \backslash \{S_\varepsilon^{(y_+)} \cup S_\varepsilon^{(y_-)}\}.$$

Finally, on the near-corner regions, e.g., $S_\varepsilon^{(x_+)} \cap S_\varepsilon^{(y_+)} \cap S_\varepsilon^{(z_+)}$, the function μ grows as a function of the distance from the vertex:

$$\mu(x,y,z) = P_4\left(\frac{r}{\varepsilon}\right), \quad r = \sqrt{(x-a+\varepsilon)^2 + (y-a+\varepsilon)^2 + (z-a+\varepsilon)^2}.$$

The construction of the function $\mu = \mu(x,y,z)$ allows one to compute the partial sources (40)–(41) using only the near-boundary values of the solution to the IP. Note that while the form of the function μ chosen for the edge and corner regions, see Fig. 7(b), may lead to an additional refraction of waves, this effect does not hamper the performance of the proposed algorithm. The reason is that we use the partition of unity (28), and the currents $\boldsymbol{j}$ and $\boldsymbol{j}^M$ are multiplied by the compactly supported function $\eta_i(t)$, see formulae (42)–(43). The modified currents (49)–(50) contain another compactly supported function $-\dot{\eta}_i(t)$. After the sources (49)–(50) cease to operate (these sources are localized inside the computational domain and do not cause the accumulation of charge), the solution inside the computational domain will become zero regardless of the spatial dependence of the quantities $\boldsymbol{j}_i(\boldsymbol{x},t)$ and $\boldsymbol{j}_i^M(\boldsymbol{x},t)$.

On the outer side of the boundary ∂S, the computational domain S is surrounded by the unsplit PML [30] that absorbs the outgoing waves. We emphasize that the PML provides a closure for the partial auxiliary problems rather than for the interior problem, whereas the closure for the IP is provided by the solution of the AP, i.e., by the sum of the solutions to the partial subproblems, see Section 8.3. At the same time, all the problems involved are coupled, and the AP, in turn, is driven by the currents derived from the solution to the IP. Maxwell's equations in the PML get modified, see [30] and [23]. The PML itself is terminated by the PEC conditions, i.e., zero Dirichlet conditions on the tangential components of the electric field.

8.2. Test solution

From the standpoint of physics, the test solution that we are going to use corresponds to the radiation of electromagnetic field by an elementary dipole antenna $d(t) = d_0\chi(t)$ located at the origin and aligned with the z axis. The signal of this antenna is modulated by the function:

$$\chi(t) = \sin^4(\omega_1 t) + \sin^4(\omega_2 t), \tag{95}$$

where the frequencies ω_1 and ω_2 will later be taken incommensurate, see Section 8.4, so that not to have a solution which is periodic in time. The resulting solution is a propagating TM that has the following non-zero components in the spherical coordinates (r,θ,φ):

$$E_r(r,\theta,t) = \psi(r)\frac{2d_0\cos\theta}{r^3}\left(\chi + \frac{\dot{\chi}r}{c}\right) - \frac{d_0\cos\theta}{r^2}\left(\chi + \frac{\dot{\chi}r}{c} + \frac{\ddot{\chi}r^2}{c^2}\right)\frac{\partial\psi}{\partial r}, \tag{96}$$

$$E_\theta = \psi(r)\frac{d_0\sin\theta}{r^3}\left(\chi + \frac{\dot{\chi}r}{c} + \frac{\ddot{\chi}r^2}{c^2}\right), \tag{97}$$

$$H_\varphi = \psi(r)\frac{d_0\sin\theta}{cr^3}\left(\dot{\chi}r + \frac{\ddot{\chi}r^2}{c}\right), \tag{98}$$

In formulae (96)–(98), the function χ and its time derivatives (denoted by upper dots) are evaluated at the retarded moment of time $t - r/c$:

$$\chi = \chi(t-r/c), \quad \dot{\chi} = \dot{\chi}(t-r/c), \quad \ddot{\chi} = \ddot{\chi}(t-r/c),$$

and

$$\psi(r) = 1 - e^{-\alpha r^5} \tag{99}$$

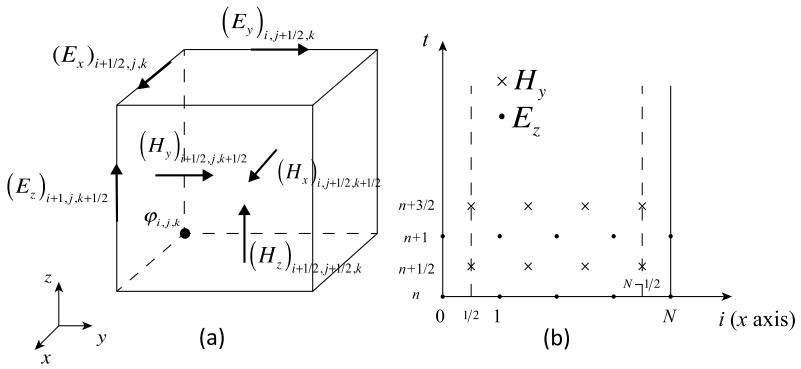

Fig. 8. (a) Allocation of the field components on the spatial grid; (b) The discretization grid in time.

is an auxiliary function needed for regularization. The fields (96)–(98) are driven by the following non-zero components of the electric current density:

$$j_r = \frac{d_0 \cos\theta}{cr^2}\left(\dot{\chi} + \frac{\ddot{\chi} r}{c} + \frac{\dddot{\chi} r^2}{c^2}\right)\frac{\partial \psi}{\partial r}, \tag{100}$$

$$j_\theta = -\frac{d_0 \sin\theta}{cr^3}\left(\dot{\chi} r + \frac{\ddot{\chi} r^2}{c}\right)\frac{\partial \psi}{\partial r}. \tag{101}$$

In other words, the fields (96)–(98) are solutions to the Maxwell equations (81)–(86) with the current densities (100)–(101) on the right-hand side.

For the factor $\psi(r)$ defined by (99), we have $\psi = \mathcal{O}(r^5)$ and $\frac{\partial \psi}{\partial r} = \mathcal{O}(r^4)$ as $r \to 0$. This behavior suppresses the singularities that would have otherwise appeared in formulae (96)–(98) and (100)–(101) at $r = 0$. On the other hand, for larger r the derivative $\frac{\partial \psi}{\partial r}$ decays very rapidly, which effectively turns the currents (100)–(101) into zero (to machine precision) outside a given finite region around the origin. By adjusting the parameter α, one can guarantee that the support of the currents (i.e., the set where the latter are non-zero) is within $S_0 = S \setminus S_\varepsilon$, see Fig. 6. This implies, in particular, that beyond this support where the Maxwell equations are homogeneous, the field (96)–(98) coincides with the true field radiated by the dipole antenna $d(t) = d_0 \chi(t)$.

The following comments are in order regarding the test solution (96)–(98):

- The fields (96)–(98) satisfy the homogeneous initial conditions $\boldsymbol{E} = \boldsymbol{0}$ and $\boldsymbol{H} = \boldsymbol{0}$.
- By design, the gradient $\operatorname{grad}\mu$ has non-vanishing r and θ components, and so does the electric field (96)–(97). Therefore, the inner product $(\operatorname{grad}\mu, \boldsymbol{E})$ in (47) is non-zero on S_ε. As such, the electric charge will, generally speaking, accumulate, and we expect to have the quasi-lacunae of the electric field. The corresponding steady-state contributions will be eliminated though by introducing the extra term (51) into the electric current (49).
- The necessary condition (61) for the existence of a divergence-free extension of the electric field is satisfied. This can be directly verified by calculating the flux of the electric field (96)–(97) through a sphere centered at $r = 0$. Physically, the flux is equal to zero because the solution is driven by a dipole-like source which is characterized by the zero total charge.
- According to (99), the domain of the interior problem roughly corresponds to $0 \leqslant r \leqslant \alpha^{-1/5}$. For the specific test solution (96)–(98) that we have chosen in the current paper, this interior problem is still fairly simple. It corresponds to Maxwell's equations with the prescribed extraneous currents. This setting can be thought of as describing the electromagnetic field radiated by the antenna with a given feed. Yet our algorithm applies to more complex problems as well, e.g., the 3D exterior scattering by complex shapes, see [31].

8.3. Implementation

Maxwell's equations are approximated by means of the well-known second order accurate Yee scheme [32], which employs a Cartesian grid and staggered discretization of the fields in both space and time, see Fig. 8. To illustrate the idea, we present the discrete counterparts of the two governing equations, (83) and (85):

$$\frac{(H_y)^{n+1/2}_{i+1/2,j,k+1/2} - (H_y)^{n+1/2}_{i-1/2,j,k+1/2}}{h_x} - \frac{(H_x)^{n+1/2}_{i,j+1/2,k+1/2} - (H_x)^{n+1/2}_{i,j-1/2,k+1/2}}{h_y}$$
$$= \frac{1}{c}\frac{(E_z)^{n+1}_{i,j,k+1/2} - (E_z)^{n}_{i,j,k+1/2}}{\tau} + \frac{4\pi}{c}(j_z)^{n+1/2}_{i,j,k+1/2}, \tag{102}$$

$$-\frac{(E_z)^{n+1}_{i+1,j,k+1/2}-(E_z)^{n+1}_{i,j,k+1/2}}{h_x}+\frac{(E_x)^{n+1}_{i+1/2,j,k+1}-(E_x)^{n+1}_{i+1/2,j,k}}{h_z}$$
$$=-\frac{1}{c}\frac{(H_y)^{n+3/2}_{i+1/2,j,k+1/2}-(H_y)^{n+1/2}_{i+1/2,j,k+1/2}}{\tau}. \tag{103}$$

The quantities h_x, h_y, and h_z in equations (102)–(103) are the grid sizes in space that we typically take equal to one another; the quantity τ is the time step that we take as $\tau = h_x/3$. When time marching the solution by means of the Yee scheme, we first advance the electric component E_z to the time level $n+1$ with the help of (102) and then update of the magnetic field to the level $n+3/2$ using (103). However, to update the near-boundary values of the magnetic field $(H_y)^{n+1/2}_{i+1/2,j+1/2,k}$, $i=0,N-1$, and $(H_x)^{n+1/2}_{i+1/2,j+1/2,k}$, $j=0,N$, one needs the electric field components $(E_z)^{n+1}_{i,j,k+1/2}$ at the boundary, i.e., at $i=0,N$ and $j=0,N-1$, respectively, see Fig. 8(b). These components are not generated by the Yee scheme itself and should rather be supplied as the boundary data. It is the AP that provides these boundary data at every time step.

The parameter ΔT of the partition of unity (28) is chosen as $\Delta T = 20\tau$. Experimentally, we have checked that it cannot be taken smaller than 10τ because otherwise the quality of the numerical lacunae will deteriorate. As for the duration T_0 of each partition element, see Fig. 5, on one hand, the longer it is the better overall efficiency one can expect (because the computational overhead will be smaller). On the other hand, an upper bound for T_0 is provided by the interval of stable performance of the chosen PML (or ABC). In the numerical simulations of Section 8.4, we have first estimated the interval of stable performance of the PML [30] experimentally, see Fig. 12, and then took T_0 equal to 0.6 of this interval (which provides a safe margin).

Due to the staggered nature of the grid used by the Yee scheme, see Fig. 8(a), there are two ways to provide a boundary closure for the IP. One can specify either the tangential components of the electric field or those of the magnetic field. In our implementation, we use the electric field.

If the boundary values of the electric field are not known, we can still update the electric field of the IP one time step further, but not on the entire grid. In our example, E_z can be updated everywhere up to the second to last node leaving the boundary nodes $i=0,N$ and $k=0,N$ undefined. Accordingly, the magnetic field H_y of the IP can be updated to next time level $n+3/2$ for all $i=3/2,\ldots,N-3/2$. This partial update is still sufficient though to create the auxiliary currents (49) and (43). Indeed, after the foregoing partial update of the fields we can compute the electric current (49) at the time level $n+1/2$, as well as the magnetic current (43) at the level $n+1$. When computing these currents, we do not need to know the non-updated boundary values of the fields because we know the exact values of currents (49), (43) at the boundary $\Gamma=\partial S$ of the computational domain S: they turn to zero there, see item 4 in the list on p. 16.

We also reiterate that we are using the original version of the magnetic current (43) without the extra term (52) because the boundary conditions for the IP involve only the electric field. In other words, it is only the electric field that is "transmitted" from the AP to IP at the boundary Γ. Accordingly, it is important that the sum (32) for the electric field should have no steady-state contributions, as the latter may potentially cause the loss of accuracy in the solution of the IP. On the other hand, in this version of the algorithm the magnetic field of the AP is of no interest as we do not transmit it to the IP. Therefore, we do not introduce the corrections (52) into the magnetic currents (50) and do not incur any additional time/memory expenses for computing the solenoidal extension of the magnetic field $\boldsymbol{H}$ from S_ϵ to S_0. In that regard we recall that the currents (49)–(50) generate one and the same cumulative solution of the AP: $\boldsymbol{w}^{\text{aux}}=[\boldsymbol{E}^{\text{aux}},\boldsymbol{H}^{\text{aux}}]^T$ regardless of whether the corrections (51)–(52) are included or not. In other words, the corrections (51)–(52) enable the no accumulation property of the partial currents (49)–(50) yet do not change the full solution of the AP, which is the sum of the partial solutions.

Of course, if we were to set the outer boundary conditions for the magnetic field rather than the electric field (see the discussion on p. 18), i.e., transmit the magnetic field from the AP to the IP, we would have built the algorithm the other way around. In other words, we would have employed the corrections (52) for the magnetic currents (50), and used no corrections for the electric currents (42). The corresponding version of the algorithm has, in fact, been tested, and the reduction of quasi-lacunae to classical lacunae has been demonstrated in practice.

Let us also emphasize that what we consider the most important development in the current paper is the modification of the electric and magnetic currents (49)–(50) by means of the corrections (51)–(52) and the divergence-free extension (57)–(58), rather than the introduction of the artificial magnetic currents (43) per se. While the magnetic currents (43) do symmetrize the Maxwell equations, which makes the overall analysis more convenient, it is the modification of the currents that transforms the quasi-lacunae of partial problems into classical lacunae (for one or both currents, depending on the specific needs) and thus removes the potential for the long-time error accumulation.

The electric current (49) with the extra term (51) requires the continuation $\boldsymbol{\mathcal{E}}$ of the electric field $\boldsymbol{E}$ onto S_0 from its boundary ∂S_0, see (53). This continuation is computed as the anti-gradient of the solution to the discretized Neumann problem (57) for the electric potential φ on S_0 (solved by FFT). The electric potential is defined at the vertices of a grid cell, see Fig. 8(a), so a new grid for φ on S_0 has to be introduced, see Fig. 9. This grid has the same dimension in each direction. The boundary values of the normal derivative of φ at ∂S_0 are taken as the values of the electric field $\boldsymbol{E}$ at the time level $n+1$ computed during the foregoing partial update.

Note that while for the current testing purposes we employ the standard FDTD discretization by means of the Yee scheme, see equations (102) and (103), there are absolutely no limitations on using the proposed algorithm with the dis-

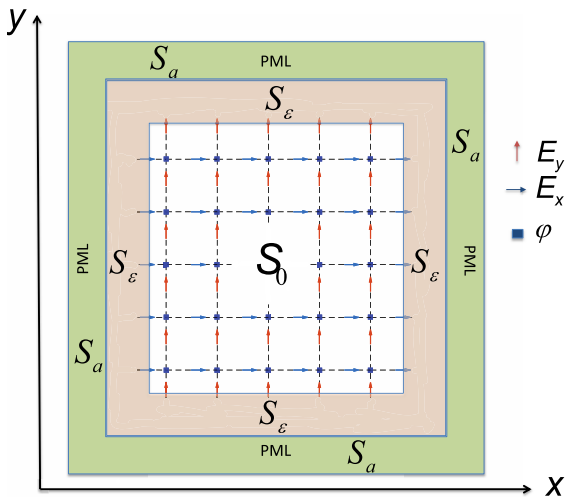

Fig. 9. Grid for the electric potential.

Table 1
The grids used in the simulations.

Grid	Grid on S	Grid on S_0	# of nodes for $S_\varepsilon^{(i)}$	# of nodes for PML, S_a
1	$36 \times 36 \times 36$	$22 \times 22 \times 22$	7	15
2	$72 \times 72 \times 72$	$44 \times 44 \times 44$	14	30
3	$144 \times 144 \times 144$	$88 \times 88 \times 88$	28	60

cretizations of other types. In fact, the lacunae-based time marching has already been successfully implemented and tested with finite volume and discontinuous Galerkin discretizations, see [33,31,34].

A block diagram of the full algorithm is presented in Appendix B, see Fig. 15. It also compares the current algorithm based on classical lacunae against its previous version [23] that was based on quasi-lacunae of Maxwell's equations.

8.4. Results of computations

In all the numerical simulations described in this section, we set the size of the domain S to $2a = 5.4$, see formula (87), and use $\alpha = 22$ in the function $\psi(r)$ of (99) to ensure that the currents (100)–(101) are well localized (to machine precision) in the ball of radius 1 centered at the origin. The frequencies that define the modulating function $\chi(t)$ of (95) are chosen incommensurate: $\omega_1 = 1$ and $\omega_2 = 1/\sqrt{2}$, so that the overall solution is not periodic.

Throughout the simulations, we use three consecutive sets of discretization grids on the spatial domains involved in the computations, see Table 1. The "Grid on S_0" in Table 1 is the grid on which the corresponding Neumann problem (57) is solved. In Table 1, we also show the number of grid nodes in the near-boundary layers $S_\varepsilon^{(i)}$, $i = x, y, z$, as well as the number of nodes in the PML S_a (adjacent to the computational domain from the outside). The partial subproblems are solved on the overall grid which combines those on S and S_a.

In Figs. 10(a)–(f), we plot the temporal evolution of the maximum norm of E_x (over the computational domain S) for the 2nd and 4th partial problems:

$$\max_S \left| E_{x,i}(t) \right|, \quad i = 2, 4. \tag{104}$$

These graphs cover a period of time from the moment $t_0^{(i)}$ when the respective subproblem starts, see (30), to the termination time $t_2^{(i)}$ when it can be dropped from the overall computation. Each graph shows two curves that correspond to the computation with the original electric current (42) that yields a quasi-lacuna and the computation with the modified electric current (49) that guarantees no accumulation of charge. In these graphs, we also plot the functions $\eta_i(t)$ that define the temporal profile of partial currents (42), (49). As we can see, in the case of the original current (42) the quantity (104) assumes a non-zero steady-state value of order one. In the case of the modified current (49), after the waves leave the computational domain the maximum field (104) rapidly approaches zero as the grid is refined. These simulations are in a very good agreement with the theoretical predictions of the current work. They demonstrate that the modified currents indeed convert the quasi-lacunae into classical lacunae (see also the discussion on superconvergence inside the lacuna at the end of this section). Similar results were obtained for all other components of the electric field.

In Figs. 11(a)–(f), we present additional numerical evidence supporting the transition from quasi-lacunae to classical lacunae rendered by the modified currents. Namely, we are showing the temporal evolution of the maximum norm of

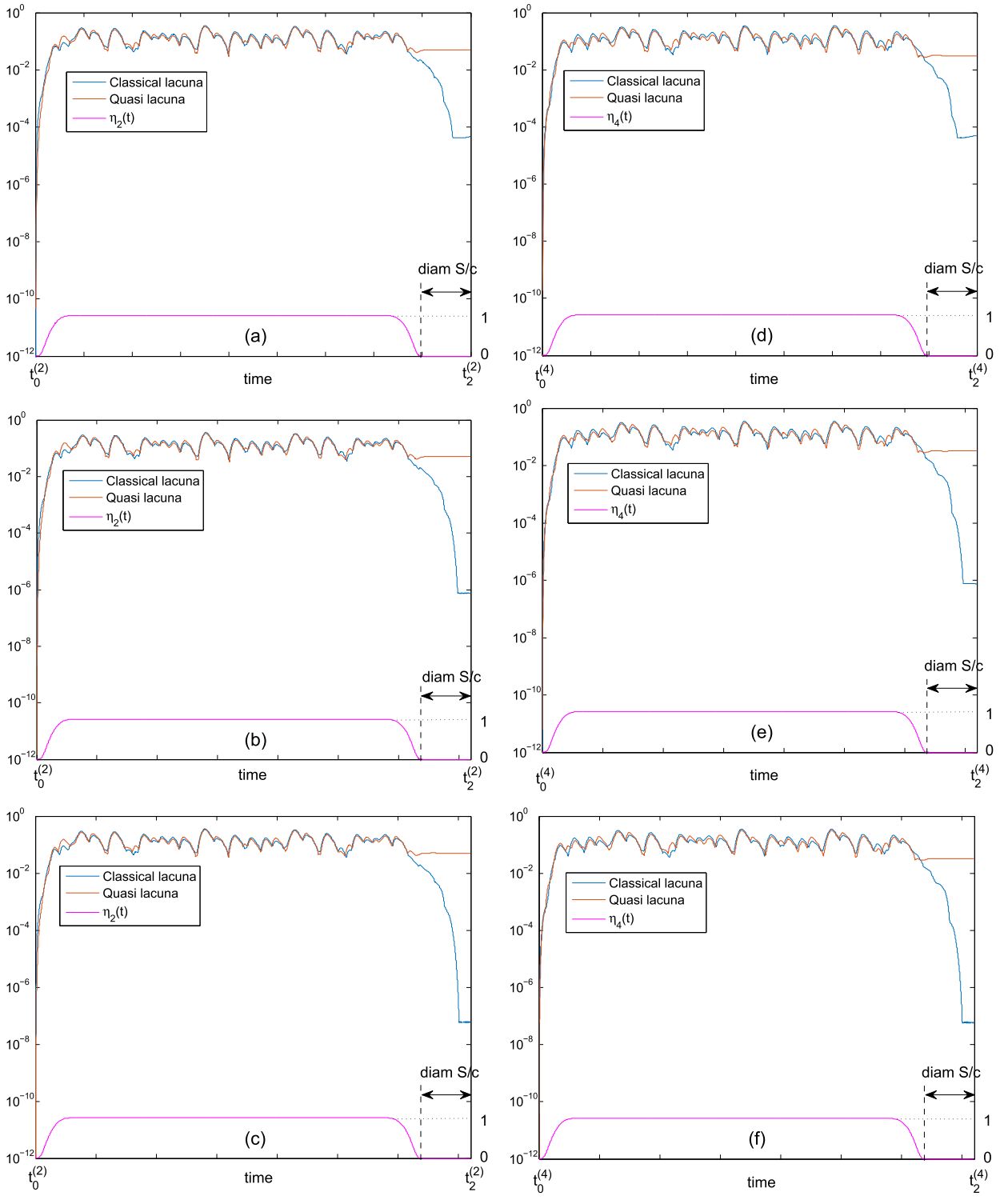

Fig. 10. Maximum absolute value of E_x (104) for the 2nd (a, b, c) and 4th (d, e, f) partial problems vs. time; the values of E_x are shown on the left vertical axis. Grids are refined from top to bottom: (a), (d) – Set 1 from Table 1; (b), (e) – Set 2; (c), (f) – Set 3. At the bottom of each panel: temporal profile of $\eta_2(t)$ or $\eta_4(t)$, respectively; the values of η are shown on the right vertical axis.

divergence of the electric field, or, according to the Gauss law (13), the L_∞-norm of the charge accumulated by the moment t:

$$\max_S |\mathrm{div}\, \boldsymbol{E}_i(t)| = \max_S |4\pi\rho_i(t)|\,, \quad i = 2, 4. \tag{105}$$

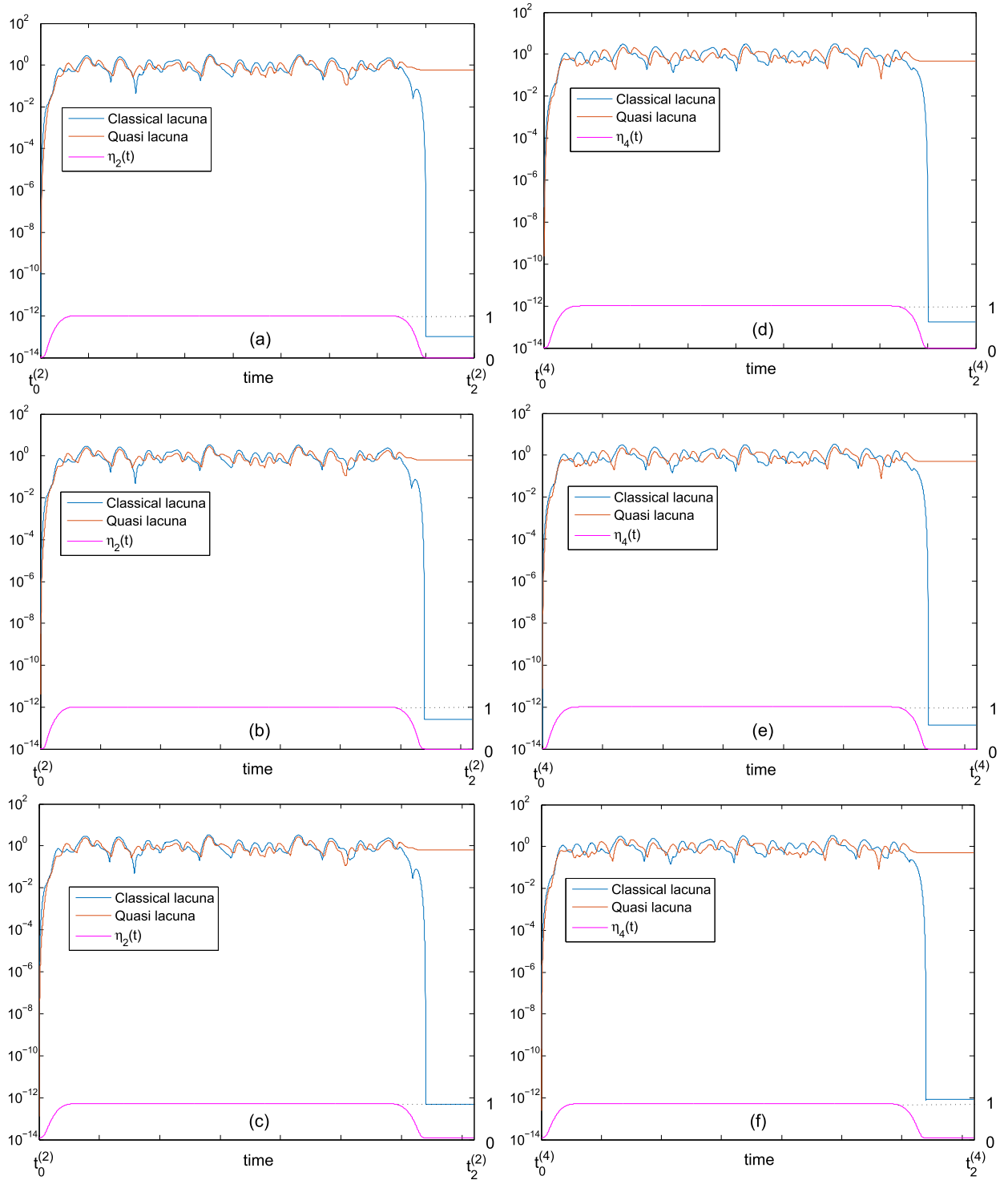

Fig. 11. Maximum absolute value of the electric charge (105) for the 2nd (a, b, c) and 4th (d, e, f) partial problems vs. time; the values of the charge are shown on the left vertical axis. Grids are refined from top to bottom: (a), (d) – Set 1 from Table 1; (b), (e) – Set 2; (c), (f) – Set 3. At the bottom of each panel: temporal profile of $\eta_2(t)$ or $\eta_4(t)$, respectively; the values of η are shown on the right vertical axis.

As before, the simulations of Fig. 11 are done for the 2nd and 4th partial problems. The graphs in Figs. 11(a)–(f) clearly indicate that the unmodified current (42) generates a non-zero accumulated charge. In contradistinction to that, the modified current (49) yields a nearly zero electric charge (to machine precision) at the end of the operation period.

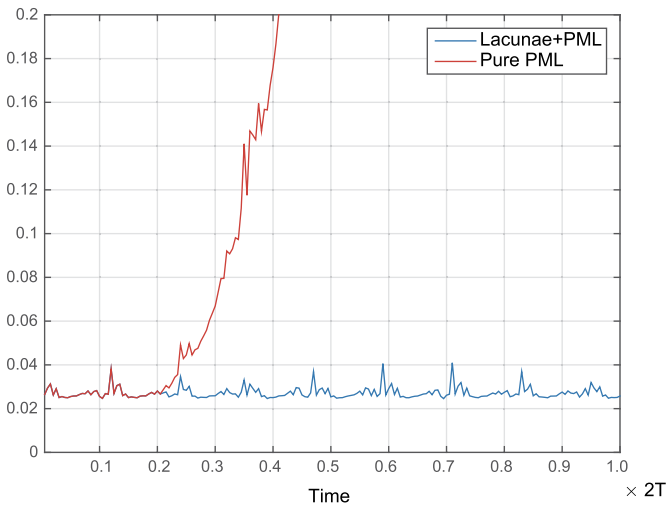

Fig. 12. The error of the component E_x vs. time in a long simulation. The PML used as a boundary closure for the interior problem causes the error to grow already at moderate times (red curve). The lacunae-based time marching algorithm removes the abrupt error growth and yields a non-increasing profile (blue curve). The computations are conducted on Grid 1 from Table 1. (For interpretation of the references to color in this figure legend, the reader is referred to the web version of this article.)

In Fig. 12, we plot the error of the numerical algorithm as a function of time in the case of the test solution (96)–(98). The error is evaluated in the maximum (L_∞) norm. For comparison, in the same plot we also present the graph that corresponds to the simulations with no lacunae-based correction. The computational domain in the latter case is terminated by the unsplit PML [30] on its own. We see that after a certain period of stable performance the error in the case of a "pure PML" begins to grow very rapidly and the solution essentially blows up. In other words, the PML employed for the simulations seems unable to maintain its stability over long simulation times. By contrast, the lacunae-based algorithm that involves the same PML (but used in short runs for partial subproblems) obviously corrects the problem. The overall computation time is very long and corresponds to nearly 2000 times required for the waves to travel across the computational domain.

Figs. 13(a–c) demonstrate the design second order grid convergence of our numerical method. Note that we use only the first two consecutive grids defined in Table 1 to study the phenomenon of grid convergence, because the computations on the finest grid (Grid 3) over long times prove too slow with the current version of the code. This issue will be addressed in the future.

Finally, from Fig. 10 one can see that the "numerical zero" inside the classical lacunae converges to actual zero far more rapidly than predicted by the design rate of the finite difference scheme (second order). This phenomenon has been noticed in some early work on the use of classical lacunae for the numerical solution of the 3D scalar wave equation (i.e., the d'Alembert equation), see [35]. It is referred to as superconvergence. In Fig. 14, we demonstrate this behavior inside the classical lacunae for Maxwell's equations. Specifically, we plot the binary logarithm of the quantity (104) at the termination time $t_2^{(2)}$ on the three grids that we employ. From the standpoint of theory, the phenomenon of superconvergence inside the lacunae is still awaiting its full explanation.

8.5. Computational complexity

As indicated in Section 6 (see p. 16), the additional computational cost of the algorithm we have proposed in the paper compared to that of [23] is not high, about 5%–10%. It is associated with the conversion of quasi-lacunae to classical lacunae. It is important to realize though that any version of the lacunae-based algorithm, whether previous [23] or current, entails an extra cost compared to the "plain" termination of the computational domain by means of an ABC or a PML. The reason is that besides the interior problem, one needs to solve an auxiliary problem. Moreover, the AP is partitioned in time and there are short time intervals on which more that one partial AP (typically, no more than two due to the appropriate choice of the parameters in (28)) need to be integrated concurrently. Altogether, a lacunae-based simulation could run about twice as slow compared to the same simulation but only with the PML. This additional expense enables a non-deteriorating performance over arbitrarily long times.

9. Conclusions

We have proposed and tested a new algorithm for the treatment of artificial outer boundaries in numerical computation of electromagnetic waves. The algorithm can help stabilize an existing ABC or PML that may otherwise produce instabilities of arbitrary nature in long-time simulations. The algorithm is universal and can be applied to a broad variety of ABCs/PMLs. It can also be used in the capacity of a standalone exact ABC that completely eliminates the error associated with the domain truncation.

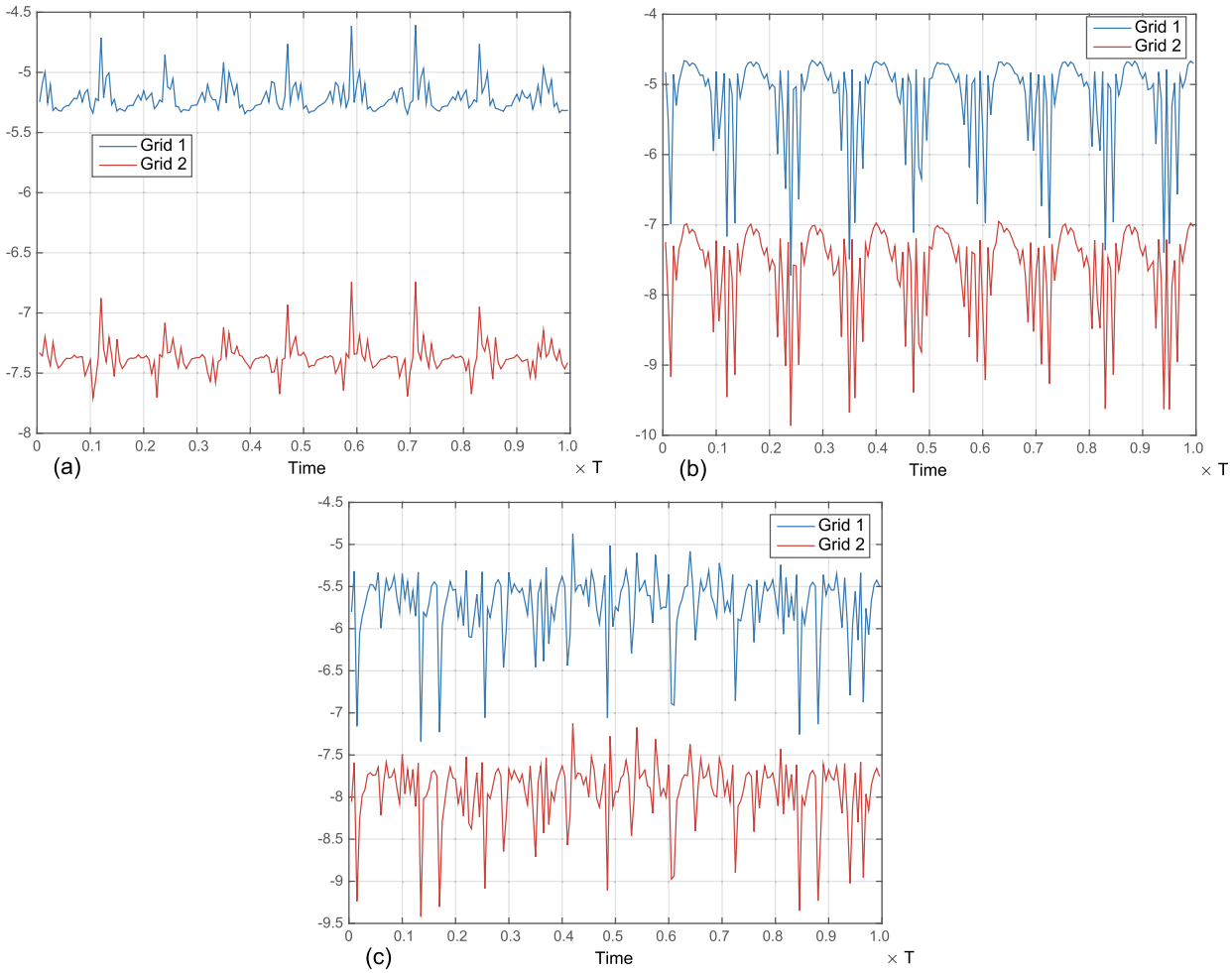

Fig. 13. Binary logarithm of the error vs. time for the field components E_x (panel (a)), E_z (panel (b)), and H_y (panel (c)). The computational time corresponds to approximately 1000 times required for waves to travel across the computational domain.

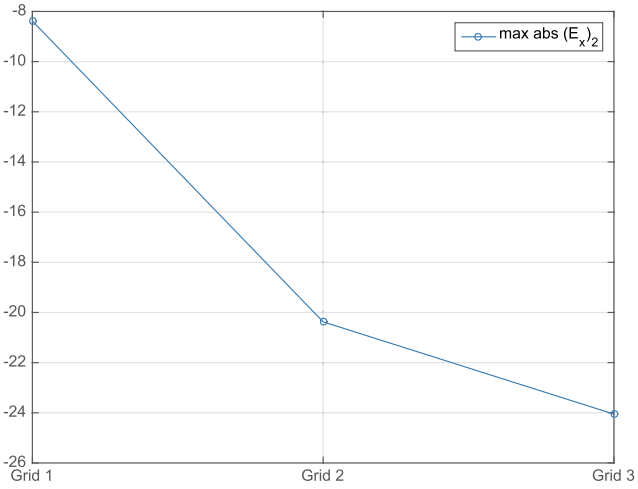

Fig. 14. Superconvergence inside the lacuna.

The algorithm is based on the Huygens' principle, i.e., the diffusionless propagation of waves and the existence of lacunae (sharp aft wavefronts) in the solutions of the governing hyperbolic PDEs. It involves two major components:

- Decomposition of the problem of interest into the interior and auxiliary problems. The interior problem accounts for the possible non-Huygens' nature of the original formulation, whereas the auxiliary problem is Huygens'. The two problems are intertwined at the outer boundary and integrated concurrently.
- The auxiliary problem consists of solving the Maxwell system of equations in vacuum driven by the specially chosen extraneous currents. It is integrated with the help of the lacunae-based time marching that suppresses the growth of any instabilities that may be associated with the given ABC or PML.

The key result of the current paper is a new approach to the time marching of the auxiliary problem. Specifically, we have been able to employ the classical lacunae for that purpose, whereas in general the Maxwell equations are characterized by quasi-lacunae. The difference is that the solution inside the classical lacunae is zero, whereas inside the quasi-lacunae it is steady-state yet not necessarily zero. The transition from quasi-lacunae back to classical lacunae required a modification of the currents that drive the auxiliary problem and the construction of a divergence-free extension of the electric and magnetic fields from the outer boundary to the interior of the computational domain. The latter question presents an independent theoretical interest.

The main benefit of using classical lacunae for the time marching is that they allow one to justify a temporally uniform bound for the error that the treatment of the artificial outer boundary introduces into the overall computation. A similar result could not be obtained under the straightforward use of the quasi-lacunae of Maxwell's equations.

The new method proposed in this paper applies to those problems that admit the aforementioned divergence-free extension of the field from the outer boundary to the interior domain. We derive the formal criteria of its applicability in terms of the flux of electromagnetic field through the outer boundary and also provide their more intuitive physical interpretation. It turns out that the resulting criteria are only very mildly restrictive.

The numerical simulations that we have conducted fully corroborate our theoretical findings. Using the modified currents, we have been able to verify that the Maxwell equations indeed acquire classical lacunae. This was done by observing the residual field behind the aft fronts, as well as the accumulated charge; both were found small. Next and most important, we have demonstrated that our method stabilizes the long-time behavior of a 3D unsplit Cartesian PML that otherwise causes the solution to blow up. Finally, we have found that the phenomenon of superconvergence inside the lacunae observed in early work on classical lacunae for the 3D wave equation also takes place for the currently redefined classical lacunae of the Maxwell equations.

Acknowledgements

We would like to thank the referees of the paper for their helpful comments and suggestions.

Appendix A. Accumulation of charge by auxiliary currents

In this section, we provide additional detail regarding the process of accumulation of charge by the partitioned currents (42)–(43) and their modified counterparts (49)–(50). To be specific, we will focus on the magnetic currents, but the results apply to the electric currents as well.

Let $t_0^{(i)}$ and $t_1^{(i)}$ denote the moments of inception and cessation of the i-th partial current, as defined by formulae (30)–(31), and let $\eta_i(t) = \zeta\,(t-(i-1)T_1)$, where $\zeta(\cdot)$ is the basic element in the partition of unity introduced in Section 4, see Fig. 5.

Lemma 1. *The charge generated by the i-th partial current (43) accumulates only when $t \in \left[t_0^{(i)}, t_1^{(i-1)}\right] \cup \left[t_0^{(i+1)}, t_1^{(i)}\right]$. These are the intervals where the function $\eta_i(t)$ is not constant and where the i-the current overlaps with the neighboring $i-1$-th and $i+1$-th currents.*

Proof. Integrating equation (48) by parts over the support of $\eta_i(t)$ and using the corresponding continuity equation from (11), we have:

$$\begin{aligned}\rho_i^M &= -\int_{t_0^{(i)}}^{t_1^{(i)}} \operatorname{div} \boldsymbol{j}_i^M dt = \frac{1}{4\pi}\,\eta_i(t)\,(\operatorname{grad}\mu, \boldsymbol{H})\big|_{t_0^{(i)}}^{t_1^{(i)}} - \frac{1}{4\pi}\int_{t_0^{(i)}}^{t_1^{(i)}} \dot\eta_i(t)\,(\operatorname{grad}\mu, \boldsymbol{H})\,dt \\ &= -\frac{1}{4\pi}\int_{t_0^{(i)}}^{t_1^{(i-1)}} \dot\eta_i(t)\,(\operatorname{grad}\mu, \boldsymbol{H})\,dt - \frac{1}{4\pi}\int_{t_0^{(i+1)}}^{t_1^{(i)}} \dot\eta_i(t)\,(\operatorname{grad}\mu, \boldsymbol{H})\,dt \equiv \rho_i^{M,0} + \rho_i^{M,1},\end{aligned} \tag{A.1}$$

where the upper dot denotes differentiation with respect to time. When integrating by parts, we took into account that $\eta_i\left(t_0^{(i)}\right) = \eta_i\left(t_1^{(i)}\right) = 0$. As $\dot{\eta}_i(t) = 0$ on that part of the entire interval $\left[t_0^{(i)}, t_1^{(i)}\right]$ where $\eta_i(t)$ is flat, we split the second integral on the first line of (A.1) into two components that correspond to the subintervals $\eta_i(t)$ increases and decreases, respectively. The resulting contributions are denoted by $\rho_i^{M,0}$ and $\rho_i^{M,1}$ on the second line of (A.1).

Thus, the total charge ρ_i^M accumulated during the operational period of the current $\boldsymbol{j}_i^M$ is the sum of the two charges that build up only when $\eta_i(t)$ varies. The charge ρ_i^M generates the steady-state field $\boldsymbol{H}_i^{\mathrm{st}}$ inside the quasi-lacuna. According to (A.1), this field also gets split into two parts that are generated by $\rho_i^{M,0}$ and $\rho_i^{M,1}$, respectively:

$$\boldsymbol{H}_i^{\mathrm{st}} = \boldsymbol{H}_i^{\mathrm{st},0} + \boldsymbol{H}_i^{\mathrm{st},1}. \tag{A.2}$$

Remark 1. The very first charge, $\rho_0^{M,0}$, is equal to zero because the initial magnetic field is zero: $\boldsymbol{H} = 0$ at $t = 0$. This can be easily verified by a calculation similar to (A.1) while taking into account that the function $\eta_0(t) = 1$ in the neighborhood of $t = 0$ by design.

Lemma 2. *Charges generated by the i-th and $i+1$-th consecutive currents during the interval of overlap $t \in \left[t_0^{(i+1)}, t_1^{(i)}\right]$ cancel each other out, i.e.,*

$$\rho_{i+1}^{M,0} = -\rho_i^{M,1}. \tag{A.3}$$

Proof.

$$\rho_i^{M,1} = -\frac{1}{4\pi}\int\limits_{t_0^{(i+1)}}^{t_1^{(i)}} \dot{\eta}_i(t)\,(\mathrm{grad}\mu, \boldsymbol{H})\,dt$$

$$= \frac{1}{4\pi}\int\limits_{t_0^{(i+1)}}^{t_1^{(i)}} \dot{\eta}_{i+1}(t)\,(\mathrm{grad}\mu, \boldsymbol{H})\,dt = -\rho_{i+1}^{M,0},$$

where we took into account that $\eta_i(t) = 1 - \eta_{i+1}(t)$ for $t \in [(i+1)T_1 - \Delta T, (i+1)T_1]$.

Equality (A.3) implies that the correspondent steady-state fields have opposite signs and cancel out one another as well:

$$\boldsymbol{H}_{i+1}^{\mathrm{st},0} = -\boldsymbol{H}_i^{\mathrm{st},1}.$$

Next, consider representation (33) of the overall solution:

$$\boldsymbol{H}(\boldsymbol{x}, t) = \sum_{i=0}^{N_0-1} \boldsymbol{H}_i^{\mathrm{st}}(\boldsymbol{x}, t) + \sum_{i=N_0}^{N_1} \boldsymbol{H}_i(\boldsymbol{x}, t),$$

and take some moment of time $t > t_1^{(N_1-1)}$ by which the latest charge $\rho_{N_1}^{M,0}$ will have already accumulated. Then, the structure of the overall accumulated charge is as follows:

$$\rho^{M,\mathrm{total}}(t) = \overbrace{\underset{\downarrow}{\rho_0^{M,0}}}^{=0} + \overbrace{\underset{\downarrow}{\rho_0^{M,1}} + \underset{\downarrow}{\rho_1^{M,0}}}^{=0} + \overbrace{\underset{\downarrow}{\rho_1^{M,1}} + \underset{\downarrow}{\rho_2^{M,0}}}^{=0} + \ldots$$

$$\ldots + \overbrace{\underset{\downarrow}{\rho_{N_1-2}^{M,1}} + \underset{\downarrow}{\rho_{N_1-1}^{M,0}}}^{=0} + \overbrace{\underset{\downarrow}{\rho_{N_1-1}^{M,1}} + \underset{\downarrow}{\rho_{N_1}^{M,0}}}^{=0} + \rho_{N_1}^{\mathrm{loc}}(t). \tag{A.4}$$

$$\underset{0}{\downarrow} \quad \underset{\boldsymbol{H}_0^{\mathrm{st},1}}{\downarrow} \quad \underset{\boldsymbol{H}_1^{\mathrm{st},0}}{\downarrow} \quad \underset{\boldsymbol{H}_1^{\mathrm{st},1}}{\downarrow} \quad \underset{\boldsymbol{H}_2^{\mathrm{st},0}}{\downarrow} \qquad \underset{\boldsymbol{H}_{N_1-2}^{\mathrm{st},1}}{\downarrow} \quad \underset{\boldsymbol{H}_{N_1-1}^{\mathrm{st},0}}{\downarrow} \quad \underset{\boldsymbol{H}_{N_1-1}^{\mathrm{st},1}}{\downarrow} \quad \underset{\boldsymbol{H}_{N_1}^{\mathrm{st},0}}{\downarrow}$$

The first term on the right-hand side of (A.4) is zero due to Remark 1. The last term on the right-hand side of (A.4) represents the residual charge generated by the last current $\boldsymbol{j}_{N_1}^H$:

$$\rho_{N_1}^{M,\mathrm{loc}}(t) = \frac{1}{4\pi}\eta_{N_1}(t)\,(\mathrm{grad}\mu, \boldsymbol{H}(t)) = \frac{1}{4\pi}(\mathrm{grad}\mu, \boldsymbol{H}(t)). \tag{A.5}$$

The quantity (A.5) depends on time and is, generally speaking, non-zero. Below each charge in formula (A.4) we have also added the respective steady-state field that it generates.

From (A.4) we can see that the successive intermediate charges cancel out one another so that

$$\rho^{\mathrm{total}}(t) = \rho_{N_1}^{\mathrm{loc}}(t). \tag{A.6}$$

This is not surprising because the charges $\rho_i^{M,0}$ and $\rho_i^{M,1}$ differ from zero only due to the non-vanishing time derivative $\dot{\eta}_i(t)$, or, in essence, due to the partition of unity. Had we introduced no partition of unity as in Fig. 5, i.e., had we set $\eta_i(t) \equiv 1$ and integrated (48) from 0 to t with the zero initial condition for $\boldsymbol{H}$, we would have obtained (A.6).

Next, let us recast the right-hand side of (33) using the two-term representation (A.2) of each steady-state field inside the computational domain:

$$\begin{aligned}&\sum_{i=0}^{N_0-1}\boldsymbol{H}_i^{\mathrm{st}}(x,t) + \sum_{i=N_0}^{N_1}\boldsymbol{H}_i(x,t)\\ &= 0 + \overbrace{\boldsymbol{H}_0^{\mathrm{st},1} + \boldsymbol{H}_1^{\mathrm{st},0}}^{=0} + \overbrace{\boldsymbol{H}_1^{\mathrm{st},1} + \boldsymbol{H}_2^{\mathrm{st},0}}^{=0} + \ldots + \overbrace{\boldsymbol{H}_{N_0-2}^{\mathrm{st},1} + \boldsymbol{H}_{N_0-1}^{\mathrm{st},0}}^{=0} + \boldsymbol{H}_{N_0-1}^{\mathrm{st},1} + \sum_{i=N_0}^{N_1}\boldsymbol{H}_i(x,t).\end{aligned} \tag{A.7}$$

Recall that the ultimate goal of the current study is to be able to disregard the sum of an increasing number of steady-state components $\boldsymbol{H}_i^{\mathrm{st}}(x,t)$ that need to be evaluated numerically and thus may cause the accumulation of error. It is clear from (A.7) though that despite the pairwise cancellation of the successive charges and the respective steady-state fields, we cannot ignore either the first sum on the right-hand side of (A.7) as a whole or any of its individual terms. Indeed, the last steady-state term on the right-hand side of (A.7), $\boldsymbol{H}_{N_0-1}^{\mathrm{st},1}$, is uncompensated and non-zero; hence it must be kept in the overall solution. This necessitates keeping the entire $\boldsymbol{H}_{N_0-1}^{\mathrm{st}} = \boldsymbol{H}_{N_0-1}^{\mathrm{st},0} + \boldsymbol{H}_{N_0-1}^{\mathrm{st},1}$, because in practice it is computed as a whole rather than separately. As such, $\boldsymbol{H}_{N_0-2}^{\mathrm{st}} = \boldsymbol{H}_{N_0-2}^{\mathrm{st},0} + \boldsymbol{H}_{N_0-2}^{\mathrm{st},1}$ should also be kept because it contains the part $\boldsymbol{H}_{N_0-2}^{\mathrm{st},1}$ that compensates $\boldsymbol{H}_{N_0-1}^{\mathrm{st},0}$. Therefore, the entire chain has to be retained, from the end to the very beginning.

The modified currents (49)–(50) differ from the original partitioned currents (42)–(43) by extra the terms (51)–(52), or, using the symbolic notation:

$$\tilde{\boldsymbol{j}}_i^M = \boldsymbol{j}_i^M + \boldsymbol{j}_i^{M,\mathrm{extra}}. \tag{A.8}$$

The current $\boldsymbol{j}_i^M$ on the right-hand side of (A.8) generates the charges $\rho_i^{M,0}$ and $\rho_i^{M,1}$ as explained previously, whereas the current $\boldsymbol{j}_i^{M,\mathrm{extra}}$ produces the same charges but with opposite signs. This can be easily verified by direct calculation. Both terms on the right-hand side of (A.8) operate concurrently, so the respective charges accumulate synchronously and compensate each other exactly at any given moment of time. Therefore, no total charge associated with the modified current (A.8) ever appears at all. Each term in the original charge decomposition (A.4) now has its own compensating counterpart provided by the same driving current $\tilde{\boldsymbol{j}}_i^M$ (specifically, by $\boldsymbol{j}_i^{M,\mathrm{extra}}$) rather than by the previous or next term in the sequence. In this sense, any individual modified current (A.8) becomes autonomous and generates zero steady-state field by itself. In other words, each of the terms $\boldsymbol{H}_i^{\mathrm{st}}(\boldsymbol{x},t)$ on the first line of decomposition (A.7) turns to zero on its own.

Yet the successive individual subproblems do not become truly independent from the standpoint of their contribution to the overall problem. The relationship between them rather takes a different form. The extra currents $\boldsymbol{j}_i^{M,\mathrm{extra}}$ generate additional fields, i.e.,

$$\boldsymbol{j}_i^{M,\mathrm{extra}} \to \boldsymbol{H}_i^{\mathrm{extra}},$$

that do not contribute to the solution of the overall problem. As we have seen, the steady-state components of these additional fields are fully compensated by the steady-state solutions generated by the genuine currents $\boldsymbol{j}_i^M$. In addition, by design $\boldsymbol{j}_i^{M,\mathrm{extra}} \propto \dot{\eta}_i(t)$, so the corresponding unsteady components of $\boldsymbol{H}_i^{\mathrm{extra}}$ and $\boldsymbol{H}_{i+1}^{\mathrm{extra}}$ generated during the interval of overlap of the two consecutive problems, i-th and $i+1$-th, exactly compensate one another too. It is important that these non-stationary components leave the computational domain once the latter falls into the lacuna, and thus can be dropped from the overall computation, i.e., replaced by their analytical value of zero.

Appendix B. Block diagram of the algorithm

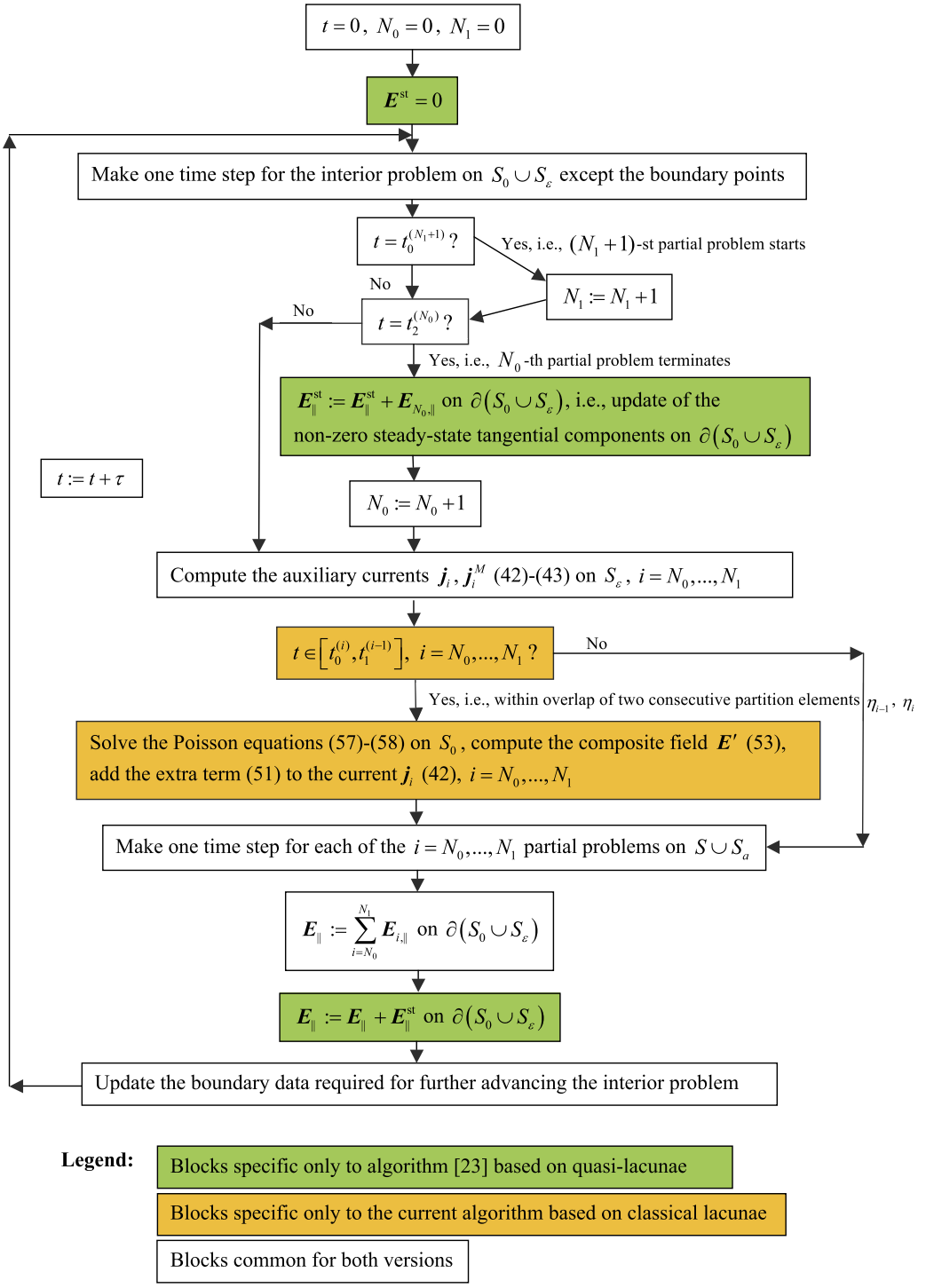

Fig. 15. Block diagram of the algorithm. $\boldsymbol{E}_\parallel$, $\boldsymbol{E}_{i,\parallel}$ and $\boldsymbol{E}_\parallel^{\mathrm{st}}$ are the tangential components of the total electric filed, i–the partial electric field, and steady-state electric field. The magnetic field is not shown for compactness. (For interpretation of the references to color in this figure, the reader is referred to the web version of this article.)

References

[1] R.L. Wagner, W.C. Chew, An analysis of Liao's absorbing boundary conditions, J. Electromagn. Waves Appl. 9 (1995) 993–1009.

[2] S. Abarbanel, D. Gottlieb, A mathematical analysis of the PML method, J. Comput. Phys. 134 (2) (1997) 357–363.
[3] O.M. Ramahi, Stability of absorbing boundary conditions, IEEE Trans. Antennas Propag. 47 (1999) 593–599.
[4] S. Abarbanel, D. Gottlieb, J.S. Hesthaven, Long time behavior of the perfectly matched layer equations in computational electromagnetics, J. Sci. Comput. 17 (1–4) (2002) 405–422.
[5] E. Bécache, P. Joly, On the analysis of Bérenger's perfectly matched layers for Maxwell's equations, M2AN Math. Model. Numer. Anal. 36 (1) (2002) 87–119.
[6] Dan Givoli, Beny Neta, High-order non-reflecting boundary scheme for time-dependent waves, J. Comput. Phys. 186 (1) (2003) 24–46.
[7] Eliane Bécache, Peter G. Petropoulos, Stephen D. Gedney, On the long-time behavior of unsplit perfectly matched layers, IEEE Trans. Antennas Propag. 52 (5) (2004) 1335–1342.
[8] Thomas Hagstrom, Timothy Warburton, A new auxiliary variable formulation of high-order local radiation boundary conditions: corner compatibility conditions and extensions to first-order systems, in: New Computational Methods for Wave Propagation, Wave Motion 39 (4) (2004) 327–338.
[9] Daniel Appelö, Thomas Hagstrom, Gunilla Kreiss, Perfectly matched layers for hyperbolic systems: general formulation, well-posedness, and stability, SIAM J. Appl. Math. 67 (1) (2006) 1–23 (electronic).
[10] Thomas Hagstrom, Stephen Lau, Radiation boundary conditions for Maxwell's equations: a review of accurate time-domain formulations, J. Comput. Math. 25 (3) (2007) 305–336.
[11] Thomas Hagstrom, Timothy Warburton, Complete radiation boundary conditions: minimizing the long time error growth of local methods, SIAM J. Numer. Anal. 47 (5) (2009) 3678–3704.
[12] Saul Abarbanel, Heydar Qasimov, Semyon Tsynkov, Long-time performance of unsplit PMLs with explicit second order schemes, J. Sci. Comput. 41 (1) (October 2009) 1–12.
[13] Thomas Hagstrom, Timothy Warburton, Dan Givoli, Radiation boundary conditions for time-dependent waves based on complete plane wave expansions, J. Comput. Appl. Math. 234 (6) (2010) 1988–1995.
[14] Daniel Rabinovich, Dan Givoli, Jacobo Bielak, Thomas Hagstrom, A finite element scheme with a high order absorbing boundary condition for elastodynamics, Comput. Methods Appl. Mech. Eng. 200 (23–24) (2011) 2048–2066.
[15] Daniel Baffet, Jacobo Bielak, Dan Givoli, Thomas Hagstrom, Daniel Rabinovich, Long-time stable high-order absorbing boundary conditions for elastodynamics, Comput. Methods Appl. Mech. Eng. 241 (244) (2012) 20–37.
[16] Thomas Hagstrom, Eliane Bécache, Dan Givoli, Kurt Stein, Complete radiation boundary conditions for convective waves, Commun. Comput. Phys. 11 (2) (2012) 610–628.
[17] Thomas Hagstrom, Dan Givoli, Daniel Rabinovich, Jacobo Bielak, The double absorbing boundary method, J. Comput. Phys. 259 (2014) 220–241.
[18] Daniel Baffet, Thomas Hagstrom, Dan Givoli, Double absorbing boundary formulations for acoustics and elastodynamics, SIAM J. Sci. Comput. 36 (3) (2014) A1277–A1312.
[19] S.V. Petropavlovsky, S.V. Tsynkov, Quasi-lacunae of Maxwell's equations, SIAM J. Appl. Math. 71 (4) (2011) 1109–1122.
[20] I. Petrowsky, On the diffusion of waves and the lacunas for hyperbolic equations, Mat. Sb. (Rec. Math.) 17(59) (3) (1945) 289–370.
[21] M.F. Atiyah, R. Bott, L. Gårding, Lacunas for hyperbolic differential operators with constant coefficients. I, Acta Math. 124 (1970) 109–189.
[22] M.F. Atiyah, R. Bott, L. Gårding, Lacunas for hyperbolic differential operators with constant coefficients. II, Acta Math. 131 (1973) 145–206.
[23] S.V. Petropavlovsky, S.V. Tsynkov, A non-deteriorating algorithm for computational electromagnetism based on quasi-lacunae of Maxwell's equations, J. Comput. Phys. 231 (2012) 558–585.
[24] V.S. Ryaben'kii, S.V. Tsynkov, V.I. Turchaninov, Long-time numerical computation of wave-type solutions driven by moving sources, Appl. Numer. Math. 38 (2001) 187–222.
[25] V.S. Ryaben'kii, S.V. Tsynkov, V.I. Turchaninov, Global discrete artificial boundary conditions for time-dependent wave propagation, J. Comput. Phys. 174 (2) (2001) 712–758.
[26] S.V. Tsynkov, Artificial boundary conditions for the numerical simulation of unsteady acoustic waves, J. Comput. Phys. 189 (2) (August 2003) 626–650.
[27] J. Hadamard, Lectures on Cauchy's Problem in Linear Partial Differential Equations, Yale University Press, New Haven, 1923.
[28] O.A. Ladyzhenskaya, The mathematical theory of viscous incompressible flow, second English edition, revised and enlarged. Translated from the Russian by Richard A. Silverman and John Chu, in: Math. Appl., vol. 2, Gordon and Breach Science Publishers, New York, 1969.
[29] A.N. Tikhonov, A.A. Samarskii, Equations of Mathematical Physics, Pergamon Press, Oxford, 1963.
[30] L. Zhao, A.C. Cangellaris, GT–PML: generalized theory of perfectly matched layers and its application to the reflectionless truncation of finite-difference time-domain grids, IEEE Trans. Microw. Theory Tech. 44 (1996) 2555–2563.
[31] A. Fedoseyev, E.J. Kansa, S. Tsynkov, S. Petropavlovskiy, M. Osintcev, U. Shumlak, W.D. Henshaw, A universal framework for non-deteriorating time-domain numerical algorithms in Maxwell's electrodynamics, in: Michail D. Todorov (Ed.), Application of Mathematics in Technical and Natural Sciences: 8th International Conference for Promoting the Application of Mathematics in Technical and Natural Sciences — AMiTaNS'16, in: AIP Conf. Proc., vol. 1773, American Institute of Physics (AIP), 2016, 020001.
[32] K.S. Yee, Numerical solution of initial boundary value problem involving Maxwell's equations in isotropic media, IEEE Trans. Antennas Propag. 14 (1966) 302–307.
[33] E.T. Meier, A.H. Glasser, V.S. Lukin, U. Shumlak, Modeling open boundaries in dissipative MHD simulation, J. Comput. Phys. 231 (7) (2012) 2963–2976.
[34] A. Fedoseyev, S. Tsynkov, E.J. Kansa, S. Petropavlovskiy, M. Osintcev, U. Shumlak, W.D. Henshaw, J. Angel, A Universal Framework for Non-deteriorating Time-Domain Numerical Algorithms in Maxwell's Electrodynamics, Final Performance Report for the US ARO STTR Contract # W911NF-14-C-0161, October 2016.
[35] V.I. Turchaninov, The gap phenomenon for solutions of the difference 3D-wave equation, Dokl. Akad. Nauk 375 (4) (2000) 451 (in Russian).